https://doi.org/10.5194/egusphere-2026-1849
Preprint. Discussion started: 9 April 2026
© Author(s) 2026. CC BY 4.0 License.

Sea ice in the Barents and Kara Seas: models versus reanalyses

Cecilia Äijälä[1], Lucía Gutiérrez-Loza[2], Wolfgang Dorn[3], Siv K. Lauvset[2], Wieslaw Maslowski[4], and Petteri Uotila[1]

[1]University of Helsinki, Institute for Atmospheric and Earth System Research / Physics, Helsinki, Finland
[2]NORCE Research, Bjerknes Centre for Climate Research, Bergen, Norway
[3]Alfred Wegener Institute, Helmholtz Centre for Polar and Marine Research, Potsdam, Germany
[4]Naval Postgraduate School, Monterey, CA, United States

Correspondence: Cecilia Äijälä (cecilia.aijala@helsinki.fi)

Abstract.

Satellite measurements indicate that the Barents and Kara Seas have experienced some of the most significant declines in sea ice concentration and an increase in sea surface temperature in the Arctic. Understanding the processes driving these changes is of utmost importance to assess the implications of climate change in the Arctic and globally. Given the observational limitations in these high-latitude areas, coupled models and reanalysis products play a key role. However, it is essential to better understand the strengths and limitations of such data products. Models are often evaluated on a pan-Arctic scale, but results might differ when considering sub-regions. This study examines two regional coupled ocean-atmosphere models (HIRHAM-NAOSIM 2.2 and RASM), two coupled model intercomparison project, phase 6 (CMIP6) models (CNRM-ESM2_1, NorESM2-MM), two regional ocean reanalyses (RARE 1.15.2 and TOPAZ 4B), one global reanalysis (ORAS5) and OSI-SAF satellite observations over the period 1991–2020. We focus on spring (March-April-May) and autumn (August-September-October) sea ice area and sea ice concentration, the edge of the sea ice, and the temperature of the mixed layer. The results show a statistically significant decrease in sea ice area and sea ice concentration in the satellite measurements and in all reanalyses. However, only one of the coupled models, HIRHAM–NAOSIM, exhibits a statistically significant sea ice decline in the Barents Sea, albeit weaker than in the reanalyses, and no coupled model shows a significant trend in the Kara Sea. Additionally, the reanalyses show a more pronounced warming of the mixed layer than the coupled models, particularly in autumn and in the Kara Sea.

1 Introduction

The Arctic sea ice is an important part of the Arctic Ocean and the global climate system, as it influences ocean circulation and atmospheric processes by regulating the exchanges of moisture, momentum and heat between the ocean and atmosphere. The reduction of sea ice has been linked to feedback mechanisms (Goosse et al., 2018) leading to Arctic Amplification (Stroeve and Notz, 2018). The two ocean basins that have experienced the largest sea ice decline and surface warming in the Arctic are the Barents and Kara Seas (Årthun et al., 2012; Lind et al., 2018; Onarheim et al., 2018) (Fig. 1). The observed warming trends in this region, along with increased salinity and altered vertical fluxes that lead to reduced stratification, have been associated with intensified Atlantic Water (AW) inflow to the Arctic, and with local and regional feedback processes, affecting both physical

https://doi.org/10.5194/egusphere-2026-1849
Preprint. Discussion started: 9 April 2026
© Author(s) 2026. CC BY 4.0 License.

and ecological systems (Asbjørnsen et al., 2020; Ingvaldsen et al., 2021). These observed changes characterise the region as a warming hotspot (Lind et al., 2018) and as a mediator of climate change between the North Atlantic and the central Arctic basins (Smedsrud et al., 2013). Furthermore, the Barents-Kara Seas warming has also been identified as a key Arctic storyline, i.e., a physically self-consistent unfolding of past or plausible future events or pathways (Shepherd et al., 2018), explaining a large proportion of the inter-model variability in pan-Arctic surface summer climate response to global warming among the Coupled Model Intercomparison Project, phase 6 (CMIP6) models (Levine et al., 2024).

The Barents and Kara Seas are shallow marginal seas of the Arctic Ocean located north of Norway and Siberia on the Siberian shelf. The average depth of the Barents Sea is 229 m, while the Kara Sea is shallower, especially in the east, with an average depth of 127 m, and 40 % of its area is less than 50 m deep. The Barents Sea is bounded by Svalbard and Franz Josef Land in the north and Novaya Zemlya in the east. The western border is towards the Greenland Sea, where warm AW flows in through the Barents Sea Opening (BSO) and later reaches the central Arctic Ocean through the Barents Sea. On the contrary, the Kara Sea is rather isolated from the adjacent seas, with Novaya Zemlya in the west as a barrier to the Barents Sea, with inflow through the Barents Sea Exit (BSX) to the north, and the shallow and narrow Kara Strait to the south. The Kara Sea is bounded to the east by Siberia and the Severnaya Zemlya archipelago, with connections to the central Arctic Ocean to the north and the Laptev Sea in the northeast. The mean annual freshwater inflow to the Kara Sea relative to its area is the largest in the world due to the inflow from the Ob, Yenisei and other large rivers, affecting its stratification and circulation patterns. These seas play distinct roles in the Arctic system — for instance, the role of the Barents Sea as a key gateway between the North Atlantic and the Arctic Ocean (Skagseth et al., 2008; Smedsrud et al., 2013) and the disproportionately large influence of the Kara Sea landfast ice on the halocline stability of the Eurasian Basin and beyond (Liu et al., 2025).

Although the Barents and Kara Seas are often studied as a single Barents–Kara region (e.g., Li et al. (2022) and Dörr et al. (2024), among others), these basins differ substantially in terms of circulation, stratification and seasonal sea ice cycle. The Barents Sea is ice-covered in the northern parts in the winter and can become nearly ice-free across the basin in summer, whereas the colder Kara Sea is typically fully ice-covered in winter and becomes largely ice-free in summer (Duan et al., 2019a, b). Observed sea ice decline has also been more pronounced in the Barents Sea than in the Kara Sea (Kumar et al., 2021). These differences motivate us to consider the two regions separately.

Advances in the observing and modelling capacities in recent decades have provided tools to widen our understanding of the polar regions. Nowadays, observations, reanalysis products and models are often used to better understand the Arctic climate system, the processes behind recent changes, and possible future storylines. Nevertheless, existing data products and models present both advantages and disadvantages. Ocean reanalyses combine models and observations via data assimilation; these products give an estimate of the ocean and sea ice (Balmaseda et al., 2015) and are important for studying processes that are only partly or indirectly observed, as well as for initialising and forcing models, even though they often struggle in data-sparse regions (Storto et al., 2019). Global Earth system models, like the Coupled Model Intercomparison Project phase 6 (CMIP6) models (Eyring et al., 2016), provide a representation of the whole Earth's climate and possible pathways for the future. However, the resolution of these models is usually too coarse to simulate all interactions and feedback between the components. Docquier et al. (2020) showed that a horizontal resolution of 1°, which is common for the global models, is not

https://doi.org/10.5194/egusphere-2026-1849
Preprint. Discussion started: 9 April 2026
© Author(s) 2026. CC BY 4.0 License.

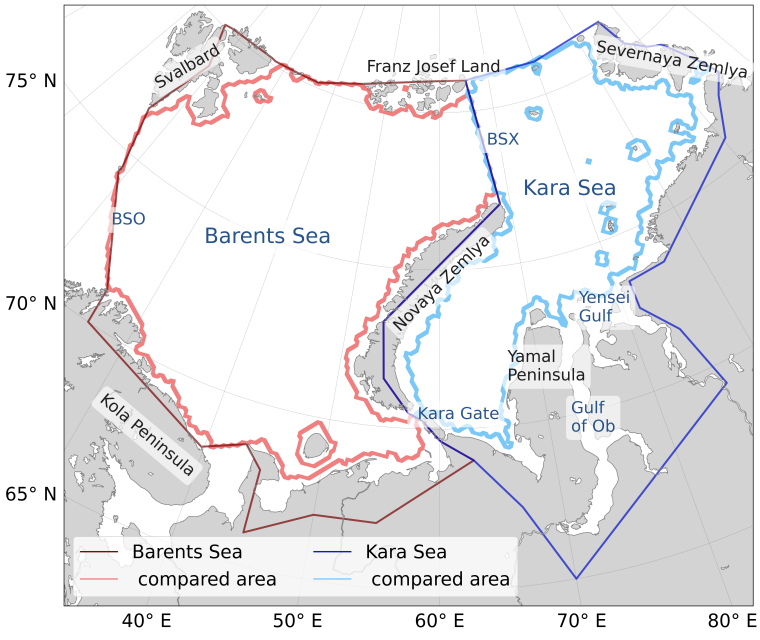


Figure 1. Barents and Kara Seas International Hydrographic Organization domains (International Hydrographic Organization and Sieger, 2012) (darker lines), and regions with data in all models (lighter colours), which are used for area-averaged comparisons. BSO stands for Barents Sea opening, and BSX for Barents Sea exit.

sufficient to correctly simulate the ocean currents entering the Arctic through the Barents Sea. Furthermore, they highlight the need for a high horizontal resolution to correctly represent the Arctic sea ice in the models. Regional coupled ocean-atmosphere models offer the ability to better resolve regional processes and associated feedbacks than their global counterparts due to their finer resolution. These models also offer the ability to respond to real-world changes in the large-scale atmospheric circulation by quasi-observed lateral boundary conditions from reanalysis data.

In this study, we investigate the capability of various global and regional reanalyses and coupled models to represent the sea ice and its recent changes in the Barents and Kara Seas. Understanding the performance of reanalysis and models in these regions is crucial due to their role as hotspots in the current Arctic climate change.

2 Data

We use data from two coupled regional atmosphere-ocean models, HIRHAM–NAOSIM (Dorn et al., 2019) and RASM (Cassano et al., 2017); two global CMIP6 (Eyring et al., 2016) Earth system models, CNRM-ESM2-1 (Séférian et al., 2019) and

https://doi.org/10.5194/egusphere-2026-1849
Preprint. Discussion started: 9 April 2026
© Author(s) 2026. CC BY 4.0 License.

Data source	Data type	Resolution (Ocean and sea ice)	Depth levels / levels $\leq$ 600 m	Period used	Ocean / sea ice models
HIRHAM–NAOSIM	Regional Model	1/12° ($\sim$ 9 km)	50 / 31	1991–2020	NAOSIM
RASM	Regional Model	1/12° ($\sim$ 9 km)	45 / 20	1991–2020	POP / CICE
NorESM	Global Model	1°	70 / 29	1991–2014	BLOM /CICE
CNRM	Global Model	1°	75 / 41	1991–2014	NEMO / GELATO
RARE	Regional Reanalysis	0.1°	75 /21	1991–2020	GFDL MOM5 / SIS1
TOPAZ	Regional Reanalysis	12.5 km	40 / 26	1991–2020	HYCOM / CICE based
ORAS	Global Reanalysis	0.25°	75 / 41	1991–2018	NEMO / LIM2
OSI-SAF	Satellite Observation	25 km	—	1991–2020	—

Table 1. Datasets used in this study.

NorESM-MM (Seland et al., 2020); data from two regional and one global ocean reanalyses, TOPAZ version 4b (Arctic Ocean Physical Reanalysis (https://doi.org/10.48670/moi-00007), RARE version 1.15.2 (Carton and Chepurin, 2023) and the global ORAS5 (Zuo et al., 2019). Additionally, we use OSI-SAF satellite sea ice concentration (SIC) data OSI-450-a (EUMETSAT, 2022) as a comparison point for the model and reanalysis data. The datasets are described below and summarised in Table 1.

2.1 Coupled Regional Models

HIRHAM–NAOSIM is a coupled regional atmosphere–ocean–sea ice model applied over a circum-Arctic domain using rotated latitude–longitude grids with a horizontal resolution of 1/4° ($\sim$ 27 km) and 40 vertical layers in the atmosphere component HIRHAM and 1/12° ($\sim$ 9 km) and 50 vertical layers in the ocean–sea ice component NAOSIM. Detailed information on the model components and their coupling is given by Dorn et al. (2019), and information on the current model version 2.2, particularly regarding recently introduced reparametrizations, is given by Aue et al. (2023) in their supplementary material. The simulation used for the present study was running for the period 1979–2021, with the first part of the simulation disregarded to let the model find its own steady state. It is driven by ERA5 reanalysis data (Hersbach et al., 2020) at HIRHAM's lateral boundaries and at HIRHAM's lower and NAOSIM's upper boundaries, which are not covered by the domain of the other model component. For NAOSIM's open lateral boundaries in the North Atlantic, ORAS5 reanalysis data (Zuo et al., 2019) were used.

RASM Cassano et al. (2017) is a fully coupled atmosphere–land–ocean–sea ice model. It uses WRF (Weather Research and Forecasting) version 3.71 for atmosphere, a regionally configured version of POP (Parallel Ocean Program) version 2.1 for the ocean and CICE (Los Alamos National Laboratory Sea Ice Model) version 6 for sea ice. Additionally, it uses the VIC (Variable Infiltration Capacity) land hydrology model and the streamflow routing (RVIC) model for transporting the freshwater flux from the land to the ocean. The ocean and sea ice have a resolution of 1/12° ($\sim$ 9 km) in a rotated grid with 45 vertical levels for the ocean, and 5 thickness categories for sea ice.

https://doi.org/10.5194/egusphere-2026-1849
Preprint. Discussion started: 9 April 2026
© Author(s) 2026. CC BY 4.0 License.

2.2 CMIP6 Earth System Models

We use two CMIP6 (Eyring et al., 2016) Earth system models, CNRM-ESM2-1 run r1i1p1f2 (hereafter CNRM) and NorESM2-MM run r1i1p1f1 (hereafter NorESM) (see Table 1). These models were chosen following the analysis described in (Levine et al., 2024), where the future simulation of CNRM represents a warm humid Arctic Ocean and cold dry continents, while NorESM represents a cold dry Arctic Ocean and warm humid continents, as described in (Mottram et. al (submitted)).

The CNRM atmosphere component is based on ARPEGE-Climat_v6.3, and run with 150 km resolution while the ocean model is NEMO (Nucleus for European Models of the Ocean) version 3.6 (Gurvan et al., 2017) which is coupled to GELATO (Global Experimental Leads and ice for ATmosphere and Ocean) sea ice model (Salas Mélia, 2002) version 6 on a grid with a nominal resolution of 1° and 75 vertical ocean layers (Séférian et al., 2019).

NorESM uses CAM6-Nor for the atmosphere, BLOM for the ocean and CICE 5.1.2 for sea ice. Both the atmosphere and the ocean are run on a 1° grid (Seland et al., 2020), and the data were provided re-gridded to 70 vertical ocean layers.

2.3 Ocean Reanalysis

The TOPAZ 4B (hereafter TOPAZ) reanalysis (Xie et al. (2017),https://doi.org/10.48670/moi-00007) is a regional ocean reanalysis for the polar region north of 50° N. It uses HYCOM (Hybrid Coordinate Ocean Model) (Chassignet et al., 2003) version 2.2 and a single category version of an early version of CICE (Xie et al., 2023) for sea ice. ERA5 (Hersbach et al., 2020) data is used as atmospheric forcing. The model uses the deterministic ensemble Kalman filter (DEnKF) to assimilate multiple ocean and sea ice observations simultaneously (Xie et al., 2023), such as SIC and drift from OSI-SAF, gridded sea surface temperature (SST) from OSTIA, and in situ temperature and salinity profiles from the CORA database. Additionally, sea ice thickness from winter months from CS2SMOS, and sea surface salinity based on the SMOS satellite are assimilated after 2010. For river runoff, the reanalysis uses a climatology based on ECMWF reanalysis and the TRIP hydrological model (Xie and Bertino, 2025). The data is provided at a standard polar stereographic grid with 12.5 km resolution and 40 depth levels.

RARE 1.15.2 (hereafter RARE) is a regional reanalysis with a southern boundary at 44.7° N Carton and Chepurin (2023). It uses the GFDL MOM5/SIS1 numerical model and ERA5 as surface forcing. The model assimilates World Ocean Database (WOD) hydrographic profiles as well as satellite and in situ SST profiles (Carton and Chepurin, 2023). Sea ice thickness estimates of PIOMAS 2.1 (Lindsay and Zhang, 2006) are used to constrain sea ice using a net surface heat flux relaxation term with a 30-day time scale, so that too thick areas compared to PIOMAS receive more surface heat flux, and too thin receives less (Carton and Chepurin, 2023). The continental discharge is based on a dataset combined from the World Meteorological Organisation Global Runoff Data Centre estimates and discharge estimates from R-ArcticNET (www.r-arcticnet.sr.unh.edu) and the Arctic Great Rivers Observatory (https://arcticgreatrivers.org/); gaps in the dataset are filled with climatological monthly estimates. The dataset is provided on a regular 0.1° Mercator grid with 75 depth levels.

ORAS5 (Ocean Reanalysis System 5, hereafter ORAS) (Zuo et al., 2019) is a global eddy-permitting ocean-sea ice ensemble reanalysis system by ECMWF. The resolution is 0.25°, and it has 75 vertical levels. ORAS is produced with the OCEAN5

https://doi.org/10.5194/egusphere-2026-1849
Preprint. Discussion started: 9 April 2026
© Author(s) 2026. CC BY 4.0 License.

system (Zuo et al., 2019), which uses NEMO V3.4 coupled to LIM2 sea-ice model and the NEMOVAR ocean assimilation system. Data assimilated includes in-situ T/S profiles from EN4 (Gouretski and Reseghetti, 2010) and SST and SIC through HadISST2 + OSTIA (Donlon et al., 2012), which is based on satellite observations.

3 Methods

In this study, we primarily analyse monthly and seasonal means and trends of ML temperature and sea ice characteristics, focusing on the spring (March, April, May, hereafter MAM) and autumn (August, September, October, hereafter ASO) seasons. These seasons are chosen because April and September correspond to the months of maximum and minimum sea ice in the Barents Sea, respectively.

The study period is 1991–2020, however, some of the datasets cover shorter periods (see Table 1), for which the available period is analysed. Monthly multiyear climatologies for each dataset are used to calculate monthly anomalies within the datasets. For these, the full period of each model has been used. The difference in the period lengths is deemed preferable to a shorter common 24 year time-period for more robust results. Analyses have also been done for the shorter common time period (not shown), without major changes to the conclusions.

Given that the regional models and reanalysis products used in this study have different grids, a bilinear interpolation was used to regrid all datasets. The equal-area 12.5 km EASE2 grid was used for this purpose. Additionally, only grid cells with data in all models were used for calculations of area averages (see Fig. 1).

3.1 Sea ice variables

For sea ice, the analysed variables are sea ice concentration (SIC), sea ice area (defined as the sum of grid-cell area multiplied by the SIC for all cells with SIC >15 %), and Integrated Ice Edge Error (IIEE, defined as the area where the model or reanalysis and OSI-SAF satellite observations disagree on the ice concentration being above or below 15 %). The IIEE is calculated following Goessling et al. (2016):

$$\mathrm{IIEE} = O + U \tag{1}$$

with

$$O = \int_A \max(c_\mathrm{m} - c_\mathrm{o}, 0)\, dA \tag{2}$$

and

$$U = \int_A \max(c_\mathrm{o} - c_\mathrm{m}, 0)\, dA\,, \tag{3}$$

where A is the area of either the Barents or Kara Seas (see Fig. 1), $c = 1$ where the sea-ice concentration is greater than 15% and $c = 0$ elsewhere. The subscript m denotes the model or reanalysis data, and the subscript o denotes the satellite observations.

https://doi.org/10.5194/egusphere-2026-1849
Preprint. Discussion started: 9 April 2026
© Author(s) 2026. CC BY 4.0 License.

3.2 Ocean variables

For the ocean, we focus on the mean temperature of the ocean mixed layer (ML). The depth of the ML is calculated for each month using the density (σ) criterion, as the depth at which the density difference to the surface (5 m) is equal to 0.03 kg m^{-3}, following the method by Sallée et al. (2006, 2013). Density at 5 m depth is used as the surface, because it is the uppermost depth available in all models. The monthly mean temperature for each grid cell is calculated for this depth. The monthly mean temperature for each region is then calculated by taking the area-weighted mean of each grid cell.

3.3 Statistics calculations

The trends are calculated using a linear least-squares regression. The statistical significance of the trends is assessed using the p-value for the null hypothesis that the regression slope equals zero. Trends are considered significant at the $p < 0.1$ level. The significance of the differences between satellite-observed sea-ice concentration and models/reanalyses, presented in section 4.3 is calculated using a Student's t-test. The Pearson's correlation coefficient, r, is used to quantify the correlation between the sea-ice area and ML temperature in section 4.4, with:

$$r = \frac{\sum_i (x_i - \bar{x})(y_i - \bar{y})}{\sqrt{\sum_i (x_i - \bar{x})^2 \sum_i (y_i - \bar{y})^2}} \,, \tag{4}$$

where $\bar{x}$ is the mean of vector x_i, and $\bar{y}$ is the mean of vector y_i. The Fishers z-test is used, with a threshold of $p < 0.05$, to determine if differences between the correlations are significant:

$$Z = \frac{z_1 - z_2}{SE} \,, \tag{5}$$

where z_1 and z_2 are calculated from r using the Fisher's transformation

$$z_n = \frac{1}{2} \ln\left(\frac{1 + r_n}{1 - r_n}\right) \quad \text{with} \quad n \in \{1, 2\} \,. \tag{6}$$

The standard error SE in (5) is given by

$$SE = \sqrt{\frac{1}{N_1 - 3} + \frac{1}{N_2 - 3}} \,, \tag{7}$$

where N_1 and N_2 represent the sample sizes of datasets 1 and 2, respectively.

4 Results

4.1 Sea Ice Area

4.1.1 Barents Sea sea ice area

The mean and trend of the sea ice area for the seasons MAM and ASO are shown in table 2. In the Barents Sea, the satellite observations from OSI-SAF indicate a mean sea ice area of 400 000 km^2 in spring (i.e., MAM) and 28 000 km^2 in the autumn

https://doi.org/10.5194/egusphere-2026-1849
Preprint. Discussion started: 9 April 2026
© Author(s) 2026. CC BY 4.0 License.

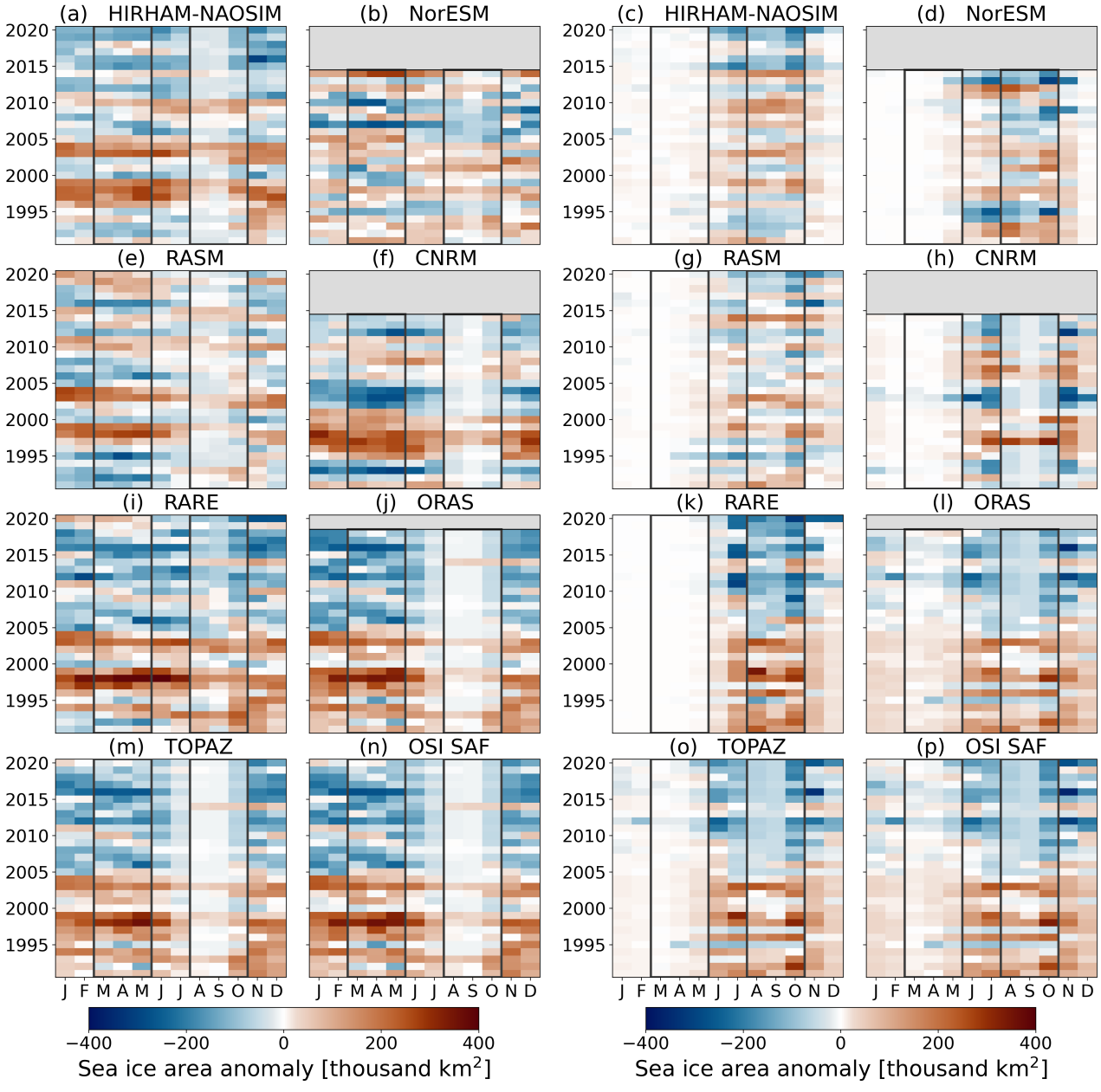


Figure 2. Sea ice area anomaly in each model for the Barents (left) and Kara Sea (right). Spring (MAM) and autumn (ASO) seasons are marked with dark grey boxes. The anomaly is calculated by taking the difference from the monthly multiyear mean for each month.

(i.e., ASO). According to the observations, the sea ice area shows statistically significant decadal trends in both seasons during

https://doi.org/10.5194/egusphere-2026-1849
Preprint. Discussion started: 9 April 2026
© Author(s) 2026. CC BY 4.0 License.

	Barents Sea						Kara Sea					
	MAM			ASO			MAM			ASO		
Model	Mean	Trend	p	Mean	Trend	p	Mean	Trend	p	Mean	Trend	p
HIRHAM–NAOSIM	611	**-44.4**	**0.059**	66	**-20.6**	**0.074**	586	-1.0	0.550	172	-13.7	0.465
RASM	534	20	0.431	61	-3.9	0.604	605	1.4	0.550	144	-20.0	0.19
NorESM	655	-0.4	0.991	117	-22.1	0.205	605	-3.5	0.292	191	-46.2	0.121
CNRM	556	-44.7	0.339	32	-10.1	0.353	605	-1.2	0.757	42	-12.6	0.561
RARE	616	**-55.0**	**0.039**	121	**-71.2**	**0.000**	624	**-1.9**	**0.001**	230	**-117.8**	**0.000**
TOPAZ	424	**-90.5**	**0.000**	30	**-24.0**	**0.000**	605	**-8.0**	**0.013**	108	**-80.6**	**0.000**
ORAS	392	**-110.6**	**0.000**	25	**-19.5**	**0.002**	580	**-15.1**	**0.006**	92	**-72.5**	**0.000**
OSI-SAF	400	**-96.2**	**0.000**	28	**-23.1**	**0.000**	586	**-15.1**	**0.002**	102	**-79.6**	**0.000**

Table 2. MAM and ASO sea ice area mean [thousand km^2], decadal trend [thousand km^2/ 10 yr], and p-value for Barents and Kara Seas. Calculated for the periods in Table 1. Trends and p-values are bold when p < 0.1.

the period 1991–2020. All reanalyses also show a statistically significant trend in both seasons in the sea ice area, while of the coupled models only HIRHAM–NAOSIM shows a statistically significant trend.

Figure 2 shows the difference between the mean sea ice area of each month and the monthly area climatology of each model. In the Barents Sea, values above the mean can be seen mostly before 2006, and values below the mean can be seen mostly after 2005 (Fig. 2n). The drop below the climatological mean coincides with winter 2005–2006, when the second-lowest April sea ice extent to date of the Barents Sea was recorded (Fig. 2n). In 2005 and 2006 the maximum sea ice area of the Arctic had two consecutive record low years, with the negative sea ice anomalies most dominant in the eastern Arctic basin (Comiso, 2006; Li et al., 2022). Regarding winter extreme sea ice areas, the minimum April extent in 2016 is shown as dark blue between February and May, while distinctly high winter values occur in 1998 and 2003.

From the ocean reanalyses, ORAS slightly underestimates the mean area in both spring and autumn, while TOPAZ slightly overestimates it, but the differences are small (Table 2). In the spring, ORAS slightly overestimates the trend and TOPAZ slightly underestimates the trend, while the opposite is true in the autumn. ORAS and TOPAZ show similar temporal patterns as OSI-SAF, which is not surprising as they assimilate OSI-SAF (Fig. 2j,m,n).

The third ocean reanalysis, RARE, shows a temporal pattern rather similar to OSI-SAF (Fig. 2i,n). Their high and low sea ice area years coincide, for example. The most notable difference is that RARE shows interannual declines in August and September, unlike OSI-SAF, ORAS and TOPAZ. This is because the mean RARE sea ice area in both spring and autumn is clearly overestimated, resulting in the largest, statistically significant decadal trend in autumn due to greater ice loss (ASO; Table 2). The trend in spring, however, is smaller than that of the other ocean reanalyses and OSI-SAF.

Of regional coupled models, the mean HIRHAM–NAOSIM spring sea ice area in the Barents Sea is close to that of RARE, and both spring and autumn mean areas are clearly higher than those of OSI-SAF (Table 2). The interannual trend in spring

https://doi.org/10.5194/egusphere-2026-1849
Preprint. Discussion started: 9 April 2026
© Author(s) 2026. CC BY 4.0 License.

in HIRHAM–NAOSIM is a lot smaller than that of OSI-SAF, even smaller than RARE, while the autumn trend is close to that of OSI-SAF. The negative anomalies are in the majority during the last ten years, signifying an interannual decline (Fig. 2a). In contrast to the three ocean reanalyses and OSI-SAF, HIRHAM–NAOSIM has an oscillating sea ice area with three above-average sea ice periods separated by periods with below-average values (Fig. 2a,i,j,m).

Of coupled models, the RASM spring mean sea ice area is the smallest, and the closest to OSI-SAF, while NorESM has the highest and the most overestimated mean area (Table 2). In autumn, the CNRM mean value is the lowest among the coupled models, with similar values to TOPAZ, ORAS, and OSI-SAF. RASM has an autumn mean close to HIRHAM–NAOSIM, and NorESM has the second-highest autumn mean after RARE. RASM shows interannual variations but no clear decadal trends (Fig. 2e).

Regarding interannual variations, CNRM shows oscillations as alternating negative and positive anomalies (Fig. 2f), while in NorESM values below average dominate around 2010. There is, however, no statistically significant trend (Fig. 2b).

4.1.2 Kara Sea sea ice area

As in the Barents Sea, the OSI-SAF, TOPAZ and ORAS sea ice areas in the Kara Sea are relatively close to each other (Table 2 and Fig. 2l, o, p). TOPAZ slightly overestimates the mean area compared to OSI-SAF in both spring and autumn, while ORAS slightly underestimates it, as was the case in the Barents Sea. Of coupled models, HIRHAM–NAOSIM has the lowest spring sea ice area, being the same as OSI-SAF. In other coupled models (RASM, NorESM and CNRM), spring sea ice areas are identical, indicating an entirely ice-covered Kara Sea (Table 2). In autumn, the CNRM mean sea ice area is unrealistically the smallest of all products analysed in this study, while other coupled models (HIRHAM–NAOSIM, RASM and NorESM) overestimate the mean autumn sea ice area compared to OSI-SAF.

In the Kara Sea, only OSI-SAF and the reanalyses show a statistically significant decreasing trend in both seasons. In spring, the sea ice area declines less than in autumn, when the TOPAZ decline is a bit less than that of ORAS and OSI-SAF (Table 2) and the RARE trend is quite small, even though it is statistically significant. In the autumn, however, the RARE trend is clearly larger than in TOPAZ, ORAS, and OSI-SAF, of which TOPAZ has the largest trend and ORAS the smallest. Moreover, RARE overestimates the mean sea ice area in spring and Autumn in the Kara Sea.

Departures from the climatological mean sea ice area in OSI-SAF, TOPAZ and ORAS are low in winter and spring (January–April), when the Kara Sea is practically completely ice-covered. The RARE monthly interannual sea ice anomaly pattern resembles OSI-SAF, TOPAZ and ORAS, even though its changes in winter appear smaller and in summer larger (Fig. 2k, l, o, p).

As in the Barents Sea, RASM does not display an evident interannual sea ice decline, and its trends are not statistically significant (Table 2 and Fig. 2g). Somewhat analogously, CNRM sea ice area in the Kara Sea oscillates inter-annually as in the Barents Sea (Fig. 2f and h). The HIRHAM–NAOSIM sea ice area decline in the Kara Sea occurred in 2015, with a clear drop in summer and autumn (Fig. 2c).

https://doi.org/10.5194/egusphere-2026-1849
Preprint. Discussion started: 9 April 2026
© Author(s) 2026. CC BY 4.0 License.

4.2 Sea Ice Edge



Figure 3. Integrated Ice Edge Error (IIEE) of the (a) Barents and (b) Kara Seas, as well as (c, d) Overestimation - Underestimation of the sea ice edge, and (e,f) time series of the yearly mean Overestimation-Underestimation. For the Kara Sea, only values during May–December are shown, as there is no ice edge during winter and spring in most years.

Given the good sea ice area agreement between ORAS, TOPAZ and OSI-SAF, it is not surprising that their integrated ice edge errors (IIEE), relative to OSI-SAF, are much smaller than those of the other datasets. Also, their monthly mean IIEEs vary relatively little (Table 3 and Fig. 3), both in the Barents Sea and in the Kara Sea. In the Barents Sea, ORAS and TOPAZ IIEEs are quite similar from July to December, while TOPAZ has a higher IIEE from January to June(Fig. 3a) due to the greater underestimation of the ice edge location than ORAS (Fig. 3c). The trend of the annual mean O-U is small for ORAS and TOPAZ and decreases over time, indicating increasing accuracy in their ice edge simulation (Fig. 3e).

After ORAS and TOPAZ, RASM has the third smallest IIEE in the Barents Sea (Table 3) with clear seasonal IIEE and O-U cycles having maxima in June and minima in September (Fig. 3a,c), which coincides with the minimum sea ice area month.

https://doi.org/10.5194/egusphere-2026-1849
Preprint. Discussion started: 9 April 2026
© Author(s) 2026. CC BY 4.0 License.

	Barents Jan–Dec				Kara May–Dec			
	IIEE	O–U			IIEE	O–U		
Model	Mean	Mean	Trend	p	Mean	Mean	Trend	p
HIRHAM–NAOSIM	237	220	**37.1**	**0.007**	123	92	**63.7**	**0.000**
RASM	142	103	**100.0**	**0.000**	87	51	**64.1**	**0.000**
NorESM	251	212	**93.4**	**0.001**	132	63	42.4	0.136
CNRM	175	54	**68.5**	**0.098**	142	-60	**59.2**	**0.081**
RARE	155	142	**19.0**	**0.006**	75	64	**11.7**	**0.018**
TOPAZ	45	-22	**12.5**	**0.000**	27	-5	**5.8**	**0.012**
ORAS	30	-19	**5.4**	**0.000**	25	-21	0.5	0.797

Table 3. IIEE mean and ice edge Overestimation - Underestimation mean, trend and p-value for Barents and Kara Sea. Means and trends are expressed in thousand km^2. Trends and p-values are bold when $p < 0.1$, indicating a significant trend. The trends are calculated from the time series shown in Figure 3 (e,f).

The RASM O-U time series shows a distinct annual trend, starting with slightly negative values and ending with values around 0.2 (Fig. 3e). This is in line with its non-significant trend in sea ice area (Table 2).

The RARE mean IIEE in the Barents Sea is only slightly larger than that of RASM (Table 3), with a similar seasonal cycle but somewhat larger monthly IIEE values due to an overestimation of the sea ice edge (Fig. 3a,c). In contrast, the RARE O-U trend is clearly smaller than that of RASM (Table 3) due to the smaller annual O-U trends after 2010 (Fig. 3e).

The ESMs have difficulties in correctly identifying the ice edge due to their coarse resolution (Table 1). Therefore, the IIEE is expected to be higher than for the other higher resolution models. The CNRM monthly IIEE in the Barents Sea is close to RARE and RASM from July to November but clearly higher in other months (Fig. 3a), as can be expected due to the coarser resolution. As for all the products, the CNRM monthly minimum IIEE occurs in September, but the monthly maximum is one month earlier, in May. Unlike most other products analysed, CNRM underestimates the ice edge from September to November and overestimates it in other months comparably moderately (Fig. 3c), resulting in a relatively small positive mean O-U (Table 3). The CNRM O-U interannual trend variability is particularly high before 2006 with big swings between negative and positive values (Fig. 3e) with strongly negative values in 1993 and 2003, coinciding with the years of low sea ice area (Fig. 2f).

The coupled models HIRHAM–NAOSIM and NorESM have the highest IIEEs and O-Us in the Barents Sea (Table 3). At least for NorESM this could be expected due to its coarse resolution. However, the monthly HIRHAM–NAOSIM IIEE is the highest among all products from October to December, with the maximum in December, although its monthly IIEE is close to those of RASM, RARE and CNRM from July to September (Fig. 3a). From January to September, the NorESM monthly IIEE is the highest, and rather close to the HIRHAM–NAOSIM monthly IIEE from April to June. The O-U trend of HIRHAM–NAOSIM is comparably small and relatively close to TOPAZ, ORAS, and RARE. This is likely associated with its declining

https://doi.org/10.5194/egusphere-2026-1849
Preprint. Discussion started: 9 April 2026
© Author(s) 2026. CC BY 4.0 License.

sea ice area over the study period (Fig. 2a). In contrast, the NorESM O-U trend is quite high, close to RASM, which has the highest O-U trend, with the sea ice edge error increasing over time (Fig. 3e).

In the Kara Sea, RARE has a slightly smaller mean IIEE than RASM in every month (Table 3 and Fig. 3b). The RARE O-U trend is small compared to the RASM, which shows the largest O-U trend among the analysed products due to its unrealistic decadal sea ice area trend (Fig. 2e). The HIRHAM–NAOSIM mean IIEE is the third-highest mean IIEE among the analysed products, with monthly values either third or second in the Kara Sea (Table 3 and Fig. 3b). It has the highest mean O-U and an exceptionally high monthly O-U in October (Fig. 3d). The HIRHAM–NAOSIM O-U trend is almost as large as in RASM, with increasing sea ice edge errors toward the end of the time series (Table 3 and Fig. 3f). The NorESM mean IIEE is the second-highest in the Kara Sea, with the highest monthly values among the products in August and September (Table 3 and Fig. 3b). From the coupled models, it is the only one that has no statistically significant O-U trend (Table 3). The CNRM coupled model has the highest mean IIEE in the Kara Sea. In contrast to the other coupled models, the CNRM mean O-U is negative, indicating more underestimation than overestimation in the ice edge (Table 3), due to underestimations from August to November (Fig. 3d), as it was seen in the ASO mean area as well (Table 2). The CNRM O-U shows large interannual variability, with a particularly low O-U value in 2003, as was the case in the Barents Sea as well (Fig. 3f).

4.3 Sea ice concentration

The SIC difference between the analysed products and OSI-SAF is shown in Fig. 4, both for the season with the maximum sea ice area (spring) and for the season with the minimum sea ice area (autumn). The decadal trends for these two seasons are shown in Fig. 5 and Fig. 6. The evolution of the SIC over the study period 1991–2020, along with the differences between the reanalysis and model products against the observed OSI-SAF concentration is discussed below.

4.3.1 Spring sea ice concentration

In spring, the OSI-SAF 1991–2020 mean sea ice edge (SIC =15%) is located at, or slightly north of the 75° N latitude until about 50° E longitude, where it turns south-west toward the southern part of the Kola peninsula (Fig. 4n and Fig. 5n). The boundary between the inner pack ice and the marginal ice zone (SIC = 80%) goes from south-east Svalbard, to the middle of the Barents Sea Exit (BSX) at the Barents–Kara Sea border between Novaya Zemlya and Franz Josef Land (see Fig. 1), and then turns south towards northern Novaya Zemlya at around 70° E. Another small area with SIC $<$ 80% exists west of Franz Josef Land. In the south, the boundary between the inner pack and the marginal ice zone is located on average on the Kara Sea side of the Kara Strait.

During the first decade, in 1991–2000, the OSI-SAF sea ice edge is somewhat south-west of the one described above, and the boundary between the inner pack and the marginal ice zone goes from southern Svalbard to northern Novaya Zemlya, and close to the Kara Strait in the south (Fig. 4n). In 2011–2020, the OSI-SAF sea ice edge location south of Svalbard has not changed much compared to earlier decades. Meanwhile, further east, the sea ice edge has clearly retreated, and touches Novaya Zemlya at around 75°N, and then goes from southern Novaya Zemlya to southern Kola peninsula (Fig. 4n). In this last decade, the SIC in the Barents Sea is generally below 80%, except in some small areas south of Franz Josef Land and east of Svalbard, while in

https://doi.org/10.5194/egusphere-2026-1849
Preprint. Discussion started: 9 April 2026
© Author(s) 2026. CC BY 4.0 License.

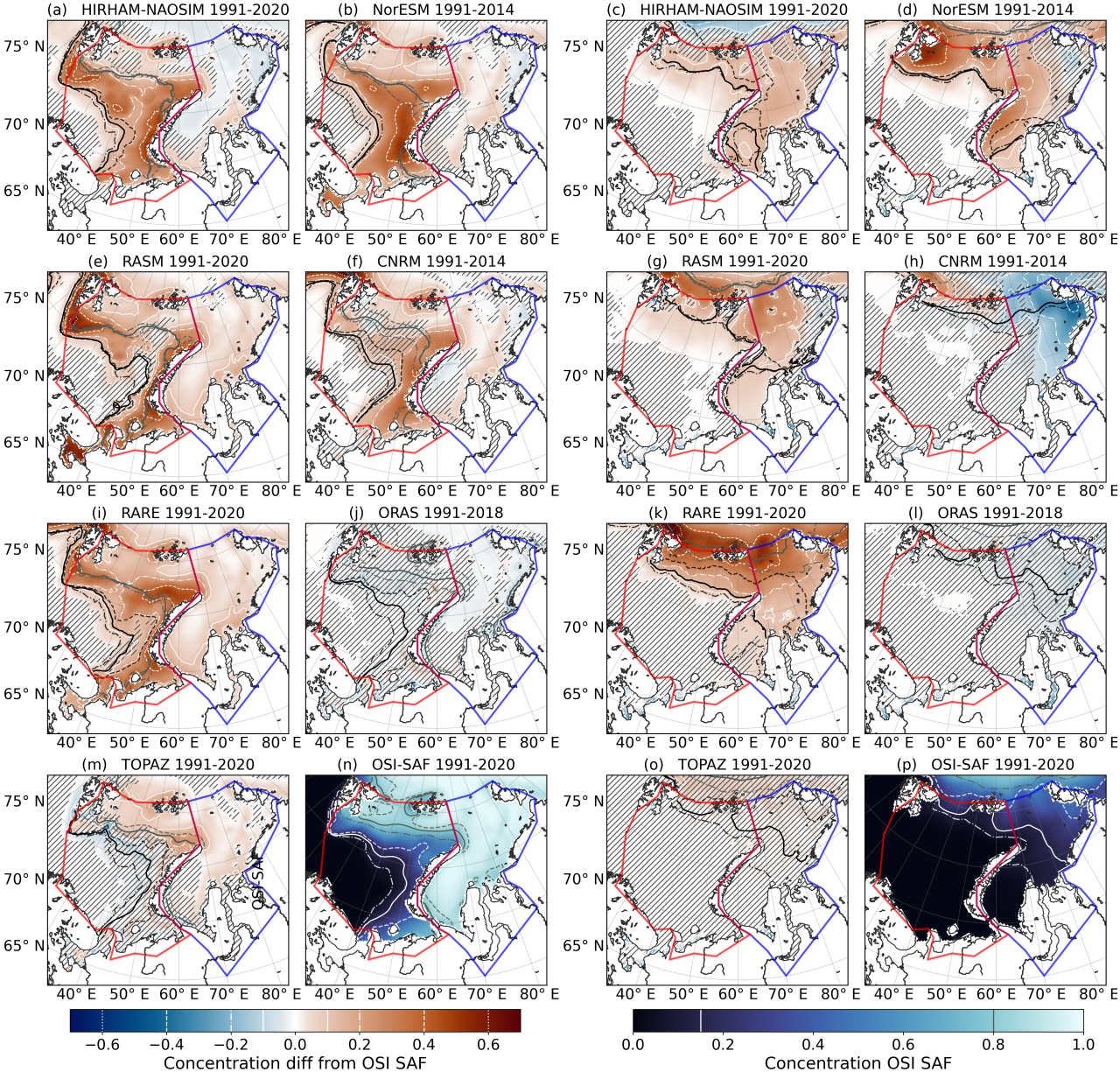


Figure 4. Mean difference between model/reanalysis and OSI-SAF sea ice concentration for MAM (left) and ASO (right), and mean OSI-SAF concentration (n and p). The difference plots (a–m, o) have been masked where the difference is not statistically significant (t-test, $p < 0.1$). The black (white) solid contour lines show the mean ice edge (SIC = 15%), and the grey contour shows the edge of the marginal ice zone (SIC = 80%) for the whole time period. To represent the sea ice edge at the start and the end of the time-series, the dash-dotted lines show the 1991–2000, and the dashed lines the mean from 2011 to the end of the dataset for the sea ice edge and the marginal ice zone.

https://doi.org/10.5194/egusphere-2026-1849
Preprint. Discussion started: 9 April 2026
© Author(s) 2026. CC BY 4.0 License.

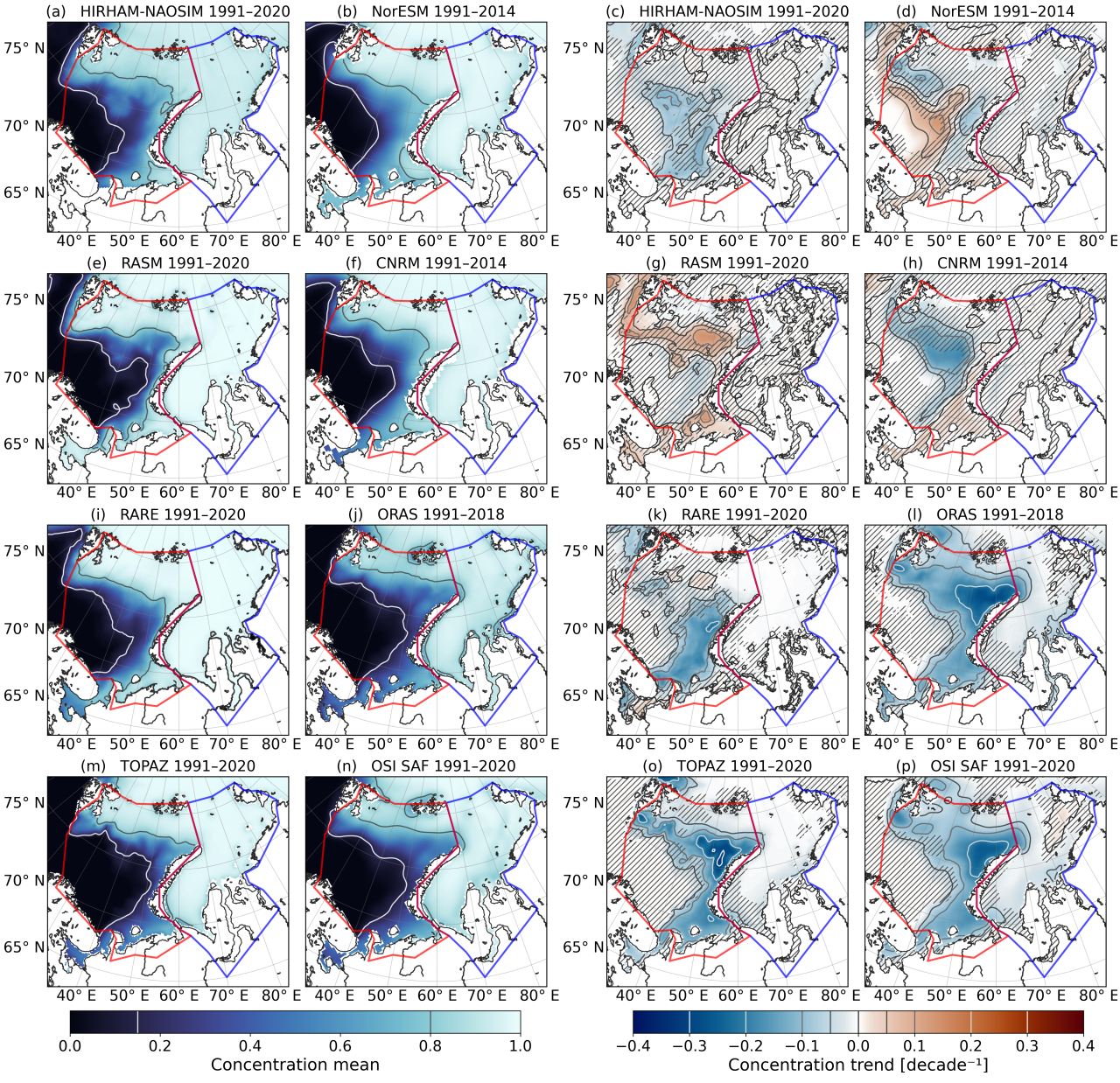


Figure 5. Average sea ice concentration mean (left) and trend (right) of all the datasets in spring (MAM) over the whole period, presented as the fraction of sea ice cover per grid cell. The mean isolines (15% and 80% ice concentration) are used to distinguish the marginal ice zone. In the trend subplots, the /// masks areas where the trend is not significant ($p > 0.1$).

https://doi.org/10.5194/egusphere-2026-1849
Preprint. Discussion started: 9 April 2026
© Author(s) 2026. CC BY 4.0 License.

the Kara Sea, the pack ice boundary has retreated at the BSX and the Kara Strait compared to earlier decades. Moreover, there is now a small marginal ice zone area north of the Yenisey Gulf.

The OSI-SAF SIC shows statistically significant negative trends for the period 1991–2020 across most of the Barents Sea ice-covered region in MAM (Fig. 5p). The negative trend is largest north-west of Novaya Zemlya, close to the region where the sea ice edge retreats at the end of the time series, where the negative trend is larger than 0.2 decade^{-1}. In the Kara Sea, the negative OSI-SAF SIC trends are smaller than in the Barents Sea, below $\pm$0.05 decade^{-1} and not always statistically significant. The small trend is mostly negative, except in the north-east, where a small area has a small positive trend. An exception to this is at the BSX, Kara Strait and north of the Yenisei Gulf, where the trends are slightly larger.

In MAM, the ORAS SIC is the closest to OSI-SAF, with no large statistically significant differences in the study area (Fig. 4j). TOPAZ overestimates SIC in the northern Barents Sea and in the Kara Sea. This, together with the IIEE underestimation (Sect 4.2), results in a narrower marginal ice zone than OSI-SAF, and a correspondingly extensive pack ice area in TOPAZ in MAM (Fig. 4m). The statistically significant overestimation tends to be larger in the Northern Barents Sea than in the Kara Sea, but is mostly less than 0.1 decade^{-1} except in the northern Barents Sea between Svalbard and Franz Josef land and north of Novaya Zemlya at the BSX (Fig. 4m). TOPAZ SIC trends form a similar spatial pattern to OSI-SAF (compare Fig. 5o and p), but with a stronger maximum negative trend west of Novaya Zemlya. In the northernmost part of the Barents Sea, however, the TOPAZ SIC trend is not significant and smaller than OSI-SAF and ORAS.

As with TOPAZ, RARE also overestimates SIC relative to OSI-SAF in MAM but with a clearly larger margin (Fig. 4i). The RARE ice edge and the boundary between the inner pack and the marginal ice zone are too extensive, and the concentration difference to OSI-SAF is statistically significant in almost the whole ice-covered region. The RARE SIC is more than 0.1 over OSI-SAF in the southern Kara Sea, in the Kara Sea at the BSX and in most of the ice-covered Barents Sea, and the difference is over 0.4 south of Svalbard and west of Novaya Zemlya. The RARE ice edge in MAM retreated eastward from 70–75° N between 1991–2000 and 2011–2020 (Fig. 4i), while the boundary between the inner pack and the marginal ice zone did not change almost at all. The RARE SIC west of Novaya Zemlya, extending toward the Kola peninsula, and the negative trend there is mostly below 0.2 decade^{-1}.

All coupled models (RASM, HIRHAM–NAOSIM, CNRM and NorESM) overestimate the MAM SIC in comparison to OSI-SAF in the Barents Sea. Furthermore, their marginal ice zones do not extend to the Kara Sea (Fig. 4a,b,e,f). RASM has the largest concentration differences compared to OSI-SAF, in particular south of Svalbard and west of Novaya Zemlya, with statistically significant differences across most of the ice-covered area (Fig. 4e). Moreover, the RASM sea ice edge and the extent of the marginal ice zone indicate limited decadal changes, as seen in previous sections.

The spring NorESM SIC is significantly higher than that of OSI-SAF, with the highest differences above 0.4 west of Novaya Zemlya (Fig. 4b). Its sea ice edge is too far west, especially south of 75°N in the Barents Sea, which explains the highest IIEE of all products (Table 3). The MAM SIC difference between OSI-SAF and CNRM is smaller than for NorESM, and broadly less statistically significant (Fig. 4g). Both products also have small areas with small statistically significant underestimations in the north-east corner of the domain and east of Novaya Zemlya.

https://doi.org/10.5194/egusphere-2026-1849
Preprint. Discussion started: 9 April 2026
© Author(s) 2026. CC BY 4.0 License.

The HIRHAM–NAOSIM sea ice edge in MAM is located too far south-west compared to OSI-SAF (Fig. 4a). The HIRHAM–NAOSIM boundary between the inner pack and the marginal ice zone are rather close to that of OSI-SAF, except it turns south at 50°E instead of continuing east, towards the Kara Sea. Also, the HIRHAM–NAOSIM pack ice boundary does not retreat between 1991–2000 and 2011–2020 as much as that of OSI-SAF. The HIRHAM–NAOSIM SIC is typically larger than OSI-SAF, especially in the marginal ice zone, except in the northern and eastern parts of the study area, and in the central Kara Sea, where HIRHAM–NAOSIM slightly underestimates sea ice concentration.

Regarding the coupled model SIC trends in MAM, NorESM and RASM show small but significantly positive trends across some quite limited regions in the Barents Sea, surrounded by large areas of non-significant trends (Fig. 5d,g). Additionally, NorESM shows some limited areas in the Barents Sea with weak but significantly negative trends. Also, HIRHAM–NAOSIM and CNRM have some limited areas with significantly negative SIC trends in the Barents Sea (Fig. 5c,h), the negative trend is stronger in CNRM than in HIRHAM–NAOSIM but the statistically significant area is much smaller. In HIRHAM–NAOSIM, the significant trend area is located in the central and southern Barents Sea, similar to the trend in RARE.

4.3.2 Autumn sea ice concentration

In autumn, the OSI-SAF SIC is above 15% in the northern part of the study area (Fig. 4p). The mean sea ice edge goes from north of Svalbard to Franz Josef Land, and from Franz Josef Land to the middle of the BSX, then continues east, and finally turns south at around 80° E (Fig. 4p). OSI-SAF shows significant negative trends in the whole ice-covered area (Fig. 6p). In 1991–2000 the sea ice edge goes from Svalbard to the northern tip of Novaya Zemlya, and then from the north-east Novaya Zemlya to the Yamal Peninsula. In comparison, the 2011–2020 mean sea ice edge goes north of the Barents Sea and along the northern boundary of the Kara Sea (Fig. 4p).

Autumn SIC between OSI-SAF and TOPAZ, and OSI-SAF and ORAS do not differ significantly (Fig. 4l,o), and the ORAS and TOPAZ decadal trends are identical to those of OSI-SAF (Fig. 6l,o). Compared to OSI-SAF, RARE overestimates the autumn sea ice edge and concentration, with the largest differences in the northern part of the study region (Fig. 4 k). The RARE mean sea ice edge goes from southern Svalbard to the northern tip of Novaya Zemlya, then continuing to the Yamal Peninsula (Fig.s 4k or 6i). The RARE region with a significant negative SIC trend resembles the corresponding OSI-SAF region. Still, it extends over a larger area in the south compared to OSI-SAF (See Fig. 6k and Fig. 6p), which is not surprising as the sea ice has a larger extent, and there is thus more ice to melt.

RASM and NorESM overestimate the average 1991–2020 SIC in autumn across the whole study region, except at some coastal locations in the Kara Sea (Fig. 4d,g). The NorESM mean sea ice edge goes further south than RASM, while the RASM mean sea ice edge goes slightly further south than that of OSI-SAF. In both models, the ice edge only retreats a bit north in the Kara Sea from 1991–2000 to 2011–2020, while no clear change can be seen in the Barents Sea.

The autumn HIRHAM–NAOSIM SIC is slightly overestimated across the entire sea ice-covered area. In the Barents Sea, the HIRHAM–NAOSIM mean sea ice edge extends too far south from Svalbard to northern Novaya Zemlya, and there is only a small ice-free area in the southern Kara Sea (Fig. 4c).

https://doi.org/10.5194/egusphere-2026-1849
Preprint. Discussion started: 9 April 2026
© Author(s) 2026. CC BY 4.0 License.

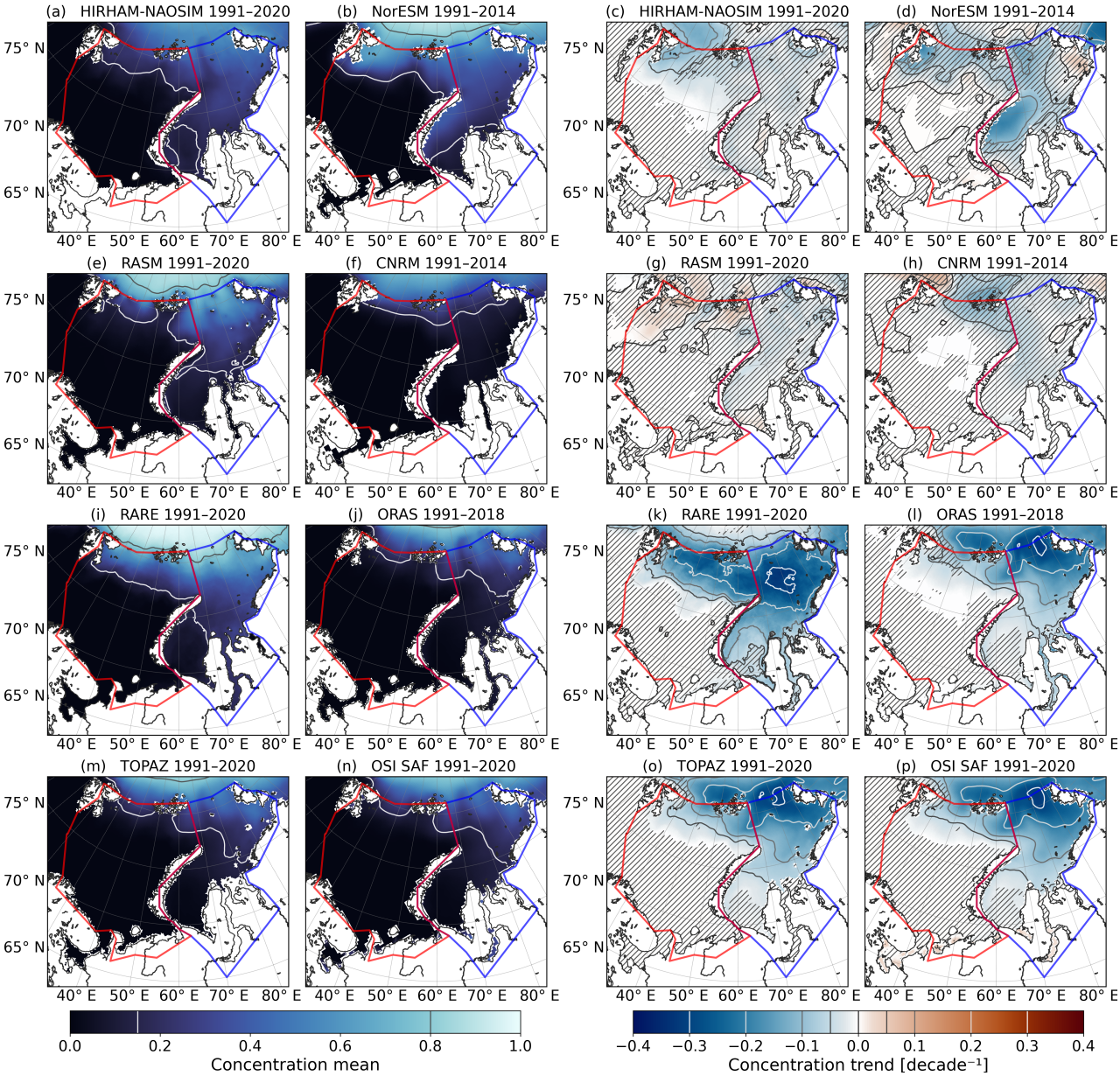


Figure 6. Average sea ice concentration mean (left) and trend (right) of all the datasets in autumn (ASO) over the whole period, presented as the fraction of sea ice cover per grid cell. The mean isolines (15% and 80% ice concentration) are used to distinguish the marginal ice zone. In the trend subplots, the /// masks areas where the trend is not significant ($p > 0.1$).

https://doi.org/10.5194/egusphere-2026-1849
Preprint. Discussion started: 9 April 2026
© Author(s) 2026. CC BY 4.0 License.

	Barents Sea						Kara Sea					
	MAM			ASO			MAM			ASO		
Model	Mean	Trend	p	Mean	Trend	p	Mean	Trend	p	Mean	Trend	p
HIRHAM–NAOSIM	-0.4	**0.23**	**0.001**	3.7	**0.56**	**0.003**	-1.7	0.00	0.323	0.1	0.23	0.207
RASM	-0.3	-0.03	0.721	3.5	0.04	0.795	-1.8	-0.00	0.321	0.1	0.21	0.132
NorESM	-0.6	-0.02	0.840	2.1	0.07	0.674	-1.7	**0.02**	**0.004**	-0.4	0.15	0.458
CNRM	-0.1	0.12	0.453	5.5	0.37	0.138	-1.8	0.01	0.412	2.3	0.32	0.455
RARE	0.7	**0.24**	**0.044**	4.3	**0.48**	**0.001**	-1.7	**-0.03**	**0.000**	1.4	**1.08**	**0.000**
TOPAZ	0.1	**0.37**	**0.000**	4.4	**0.65**	**0.000**	-1.7	**0.01**	**0.001**	1.5	**1.04**	**0.000**
ORAS	0.1	**0.37**	**0.000**	4.2	**0.77**	**0.000**	-1.7	-0.00	0.348	1.4	**0.93**	**0.000**

Table 4. MAM and ASO mean ML temperature [°C], decadal trends [°C/ 10 yr] , and p-values for Barents and Kara Seas. Calculated for the maximum period of each dataset. Trends and p-values are bold when $p < 0.1$.

In CNRM, the mean SIC does not differ significantly from OSI-SAF in the Barents Sea in ASO. In contrast, in the Kara Sea, the SIC is clearly underestimated (Fig. 4h). The CNRM mean sea ice edge goes from Svalbard to the BSX, and continues eastward towards the south of Severnaya Zemlya.

The coupled model autumn sea ice area and concentration trends are not significant, with few exceptions (see Table 2 and Fig. 6c,d,g,h). In a small area east of Svalbard, HIRHAM–NAOSIM has a statistically significant negative SIC trend (Fig. 6c), and the NorESM negative SIC trend is statistically significant in an area east of Novaya Zemlya and in a small area at the east coast of Svalbard (Fig. 6d).

4.4 Ocean temperature of the mixed layer

The mean temperature and trends of the ML are shown in Table 4 for the seasons MAM and ASO. In the Barents Sea, the spring (MAM) mean temperature varies from −0.6 °C (NorESM) to 0.7 °C (RARE) between the models. The mean ML temperature in the regions stays mostly below 5 °C, except in NorESM and RARE, where some warmer waters can be seen (Fig. A1c,i). In the Kara Sea, the MAM variation is smaller, and the ML is close to freezing (Table 4). In autumn (ASO), the ML temperature in the Barents Sea is between 2.1 (NorESM) and 5.5 °C (CNRM), and between −0.4 (NorESM) and 2.3 °C (CNRM) in the Kara Sea. The mean ML temperature stays mostly below 10 °C in the Barents Sea, except in the south-west in RASM, CNRM and RARE (Fig. A2e,f,i), and mostly below 5°C in the Kara Sea, except in the south-west in RASM, CNRM, RARE and TOPAZ (Fig. A2e,f,i,).

The ML temperature trend is positive and statistically significant in the Barents Sea in both MAM and ASO for the reanalyses and for HIRHAM–NAOSIM, being stronger in the autumn (Table 4). In MAM the warming trend is highest IN HIRHAM-NAOSIM, ORAS and TOPAZ in the ice free areas, or close to the ice edge (Fig. A1c,l,o) while in RARE the highest warming coincides with the areas of strong decreasing SIC trend in the marginal ice zone (Fig. 5k and A1k). In RASM, NorESM and

https://doi.org/10.5194/egusphere-2026-1849
Preprint. Discussion started: 9 April 2026
© Author(s) 2026. CC BY 4.0 License.

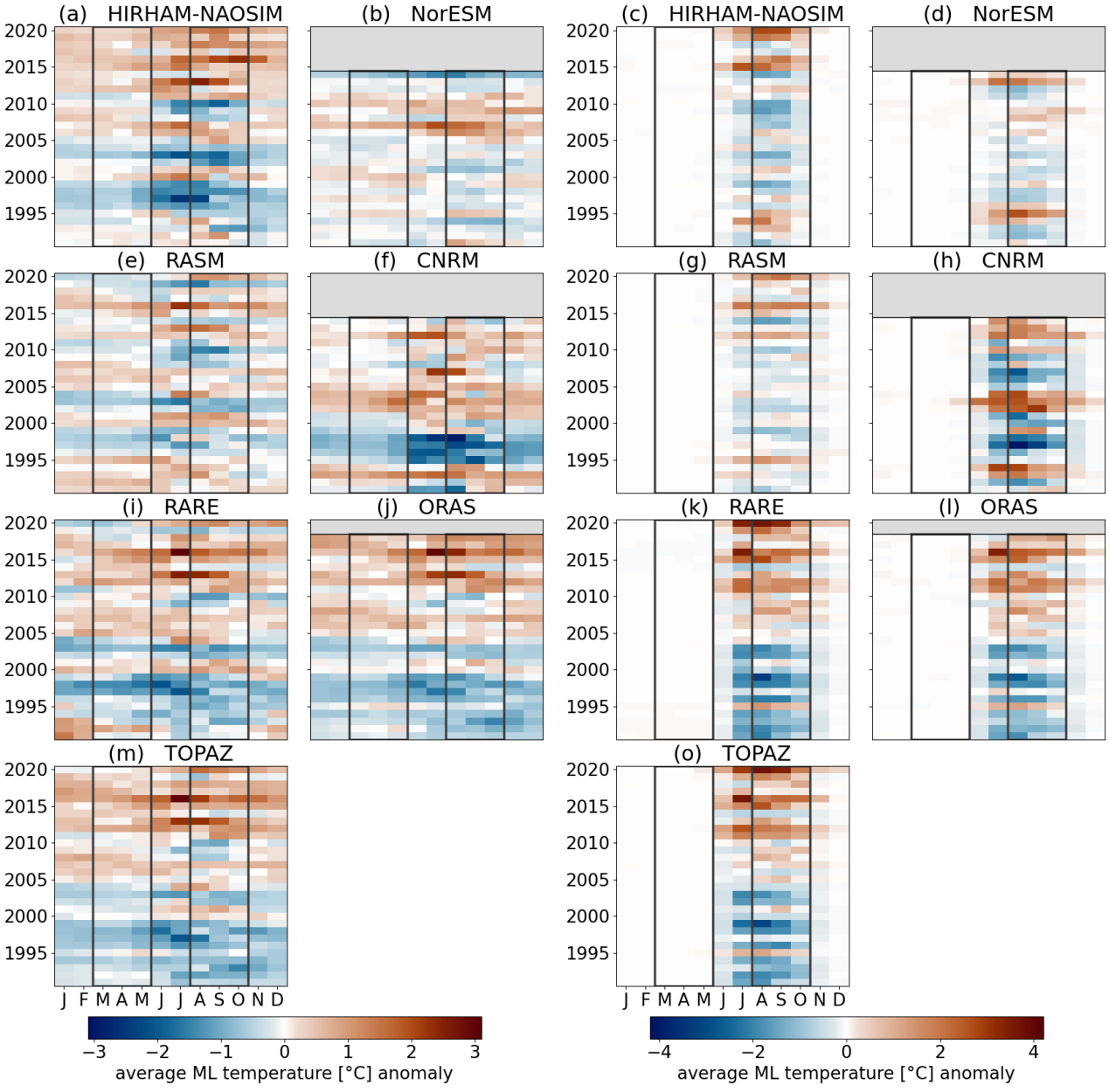


Figure 7. ML temperature anomaly in each model for the Barents (left) and Kara Sea (right). Spring (MAM) and autumn (ASO) seasons are marked with dark grey boxes. The anomaly is calculated by taking the difference from the monthly multiyear mean for each month. Note the different colour scales in the figures.

https://doi.org/10.5194/egusphere-2026-1849
Preprint. Discussion started: 9 April 2026
© Author(s) 2026. CC BY 4.0 License.

	Barents Sea				Kara Sea			
	Whole year		APR–SEP	OCT–MAR	Whole year		APR–SEP	OCT–MAR
Model	r	r_{diff}	r_{diff}	r_{diff}	r	r_{diff}	r_{diff}	r_{diff}
HIRHAM–NAOSIM	-0.903	-0.681	-0.648	**-0.832**	-0.912	-0.766	**-0.837**	**-0.855**
RASM	-0.917	-0.631	-0.553	**-0.819**	-0.936	-0.676	-0.642	**-0.838**
NorESM	-0.932	-0.722	-0.695	**-0.807**	-0.907	-0.783	-0.816	**-0.910**
CNRM	-0.838	-0.702	-0.676	**-0.820**	-0.873	-0.664	-0.747	-0.726
RARE	-0.891	-0.794	-0.788	-0.840	-0.942	-0.864	**-0.916**	**-0.927**
TOPAZ	-0.885	-0.690	**-0.568**	**-0.877**	-0.899	-0.663	-0.704	**-0.828**
ORAS	-0.858	-0.672	**-0.546**	**-0.836**	-0.901	-0.668	-0.735	**-0.768**

Table 5. Pearson's correlation coefficients between sea ice area and ML temperature of Barents and Kara Sea, denoted as r, and between the sea ice area anomaly (Fig. 2) and ML temperature anomaly (Fig. 7), denoted as r_{diff}. r_{diff} is calculated both for the monthly data of the whole year and for the summer (APR–SEP) and winter (OCT-MAR) half years separately. Bold numbers are statistically significantly different from full year r_{diff} using Fisher's z-test ($p < 0.05$)

CNRM, the Barents Sea trend is not significant. In the Kara Sea, the trend is small for all models in spring, when the region is ice-covered (Table 4). In Autumn, the trend is statistically significant in the reanalyses and close to 1 °C/decade (Table 4). The ASO ML temperature trend is clearly stronger in the Kara Sea than in the Barents Sea in all the reanalyses. The Kara Sea average ML temperature is smallest in ORAS (Table 4), where the trend is below 1 °C/decade north of 75° N, but strongest of all reanalyses at the cost, being over 2 °C/decade in some areas (Fig. A2l). In RARE and TOPAZ, the above 1 °C/decade warming is more widespread and covers most of the area, except the north, being somewhat broader and stronger in RARE (Fig. A2k,o).

Figure 7 shows the ML temperature anomaly (difference between monthly mean and monthly climatology) and Table 5 shows the Pearson's correlation coefficient (PCC) calculated between sea ice area and ML temperature and between the anomalies (shown in Fig. 2 and 7). The temperature follows similar patterns to that of the sea ice area (Fig 2), discussed in Section 4.1.1 and 4.1.2. The reanalyses show a decline with 2005–2006 showing a switch from mainly below average and above average temperatures in both regions, though in the Kara Sea, the year-to-year variations are mainly seen in summer and autumn (for all models). RASM has only year-to-year variation, in both regions, with no trend. Some oscillation is present in HIRHAM–NAOSIM in the Barents Sea and in CNRM in both regions, as seen in the sea ice area (section 4.1.1). The correlation coefficient (r) (Table 5) between the sea ice and temperature is negative for all datasets, and between -0.83 and -0.94, and the correlation coefficient between the anomalies (r_{diff}), where the effect of the annual variation is removed, is between -0.63 and -0.86 for all datasets. The correlation coefficient between the anomalies is higher in the Kara Sea than in the Barents Sea for all datasets except CNRM and TOPAZ. When calculating correlation coefficients between the anomalies (r_{diff}) for the light summer (Apr–Sep) months and dark winter months (Oct–Mar) separately, the correlation coefficient for

https://doi.org/10.5194/egusphere-2026-1849
Preprint. Discussion started: 9 April 2026
© Author(s) 2026. CC BY 4.0 License.

winter is always higher than for the full year for all datasets for both regions. This difference is statistically significant using Fisher's z-test ($p < 0.05$) for all datasets except for RARE in the Barents Sea and CNRM in the Kara Sea, and only CNRM in the Kara Sea has a summer value slightly higher than the winter value. In the Barents Sea, the correlation coefficient for summer is always smaller than that for the whole year, but the difference is only statistically significant for TOPAZ and ORAS. In the Kara Sea, only RASM shows a lower correlation coefficient for summer than for the whole year, and most differences for the whole year are statistically not significant.

5 Discussion and Conclusions

Coupled models and reanalyses were evaluated against OSI-SAF satellite measurements regarding their performance in representing the sea ice in the Barents and Kara Seas. The satellite measurements show a significant decreasing trend in the sea ice area in the Barents and Kara Seas in both MAM and ASO. The trend is larger in the Barents Sea in MAM than in ASO, and larger in the Kara Sea in ASO than in MAM. This is because the Kara Sea is still mostly fully ice-covered in MAM, while in ASO the two regions, but especially the Barents Sea, are already mostly ice-free at the end of the study period. The decreasing trends seen here agree with previous studies (e.g., Duan et al., 2019b; Kumar et al., 2021; Liu et al., 2022; Shabanov et al., 2024).

The reanalyses examined show significant decreasing trends in sea ice area and concentration as well. From the coupled atmosphere-ocean models, however, only HIRHAM–NAOSIM shows a statistically significant decreasing trend in the Barents Sea ice area, but on a lower level of significance than the satellite data and the reanalyses. Also, the regions with significant trends in sea ice concentration are smaller. In the Kara Sea, none of the coupled models show a statistically significant change.

Mean sea ice area is overestimated in most of the coupled models and in the RARE reanalysis due to both an overestimation of the concentration and a shifted location of the ice edge. CNRM is an exception, as it underestimates the sea ice, especially in the Kara Sea in ASO. TOPAZ and ORAS mean sea ice area and sea ice edge are closest to the satellite measurements, which is not surprising, as they assimilate satellite data. However, TOPAZ tends to overestimate the sea ice concentration in spring, while ORAS slightly underestimates the Kara Sea ice concentration. Even though RARE does not assimilate satellite data, it is able to produce a negative trend, but its mean sea ice area is higher than in the other reanalyses. This indicates that data assimilation has a strong impact on the skill to represent the sea ice correctly, as shown in previous comparisons of Arctic reanalysis products and prediction systems (e.g., Zhang et al., 2021; Xiong et al., 2025), and it is consistent with documented inter-reanalysis differences arising from different assimilation strategies (see Uotila et al., 2019). Thus, while TOPAZ and ORAS provide a useful reference for the coupled ocean–sea ice state and its variability, their high skill in sea ice primarily reflects the impact of assimilation, and does not necessarily indicate superior physical process representation compared to the free-running coupled models. Even though reanalyses are important tools and sources of data for research, they can not be used for everything (Storto et al., 2019).

For coupled atmosphere-ocean models, it can not be expected that the results follow observations exactly, as they represent a possible pathway of the climate system rather than a direct reproduction of observed conditions. Although coupled regional

https://doi.org/10.5194/egusphere-2026-1849
Preprint. Discussion started: 9 April 2026
© Author(s) 2026. CC BY 4.0 License.

models can be driven by quasi-observed data at the lateral boundaries, the simulation inside the model domain evolves freely. Consequently, small differences in the initial state can lead to different simulation results. Their goal is to simulate realistic climate dynamics and to reproduce statistical properties of the climate. From the coupled models, RASM has the smallest IIEE, with results close to those of RARE. However, as mentioned before, there is no trend in the sea ice area, while the ice edge overestimation-underestimation shows the largest trend, because the ice edge does not move during the study period. On the other hand, HIRHAM–NAOSIM shows a large IIEE with the largest overestimation-underestimation in the Barents Sea. Trend-wise it is the best performing model in the Barents Sea, while it does not perform better than the other models in the Kara Sea. This might have to do with the differences between the basins, the dominant physical processes, and how well they are represented in the models.

Several studies have looked into the sea-ice variability in the Barents and/or Kara Seas and the processes behind it (e.g., Duan et al., 2019a; Kumar et al., 2021; Li et al., 2022; Shabanov et al., 2024; Chatterjee et al., 2024; Dörr et al., 2024). Warm Atlantic waters flow into the Barents Sea through the BSO, where the water cools and mixes, releasing heat into the atmosphere. Part of this modified water continues into the Kara Sea through the BSX and Kara Gate. Shabanov et al. (2024) stated that the warm water inflow is the most important process for the sea ice decline in the Kara Sea. While this oceanic inflow can enhance sea-ice melt and contribute to Atlantification, several studies (e.g., Liu et al., 2022) showed that atmospheric forcing can dominate interannual to decadal sea-ice variability, with air temperature, winds, and radiative fluxes exerting strong control. Recent work also indicates that the relative importance of these drivers varies spatially (Dörr et al., 2024). Overall, the atmosphere, ocean, and sea ice form a tightly coupled system, and internal feedbacks make it difficult to attribute observed variability to any single driver (Duan et al., 2019a; Chatterjee et al., 2024).

The temperature of the ML tells a similar story as the sea ice. A statistically significant increasing trend of the mean ML temperature can be seen in the Barents Sea in both MAM and ASO for the reanalyses and HIRHAM–NAOSIM, while in the Kara Sea, a clear statistically significant trend can only be seen in the reanalyses in ASO. The correlation between the sea ice area anomaly and the ML temperature anomaly is high in all datasets, which is in line with previous studies (Kumar et al., 2021; Li et al., 2022). There is no clear difference between the different classes of datasets (models vs. reanalyses), even though there is some variation between the datasets. RARE seems to have a somewhat higher correlation between the anomalies than TOPAZ and ORAS, but more research would be needed to see if this difference is significant. The mean ML temperatures between the reanalyses are also quite similar, although the magnitude and spatial pattern of the autumn trend differ between them. Taken together, the consistently high correlations indicate that oceanic conditions play an important role in shaping the sea-ice variability, even if atmospheric processes are not explicitly examined here. This makes it particularly important to investigate the ocean component of the coupled models to understand why they fail to reproduce the observed warming in the Kara Sea, and for most of them also in the Barents Sea.

It was shown by Yamagami et al. (2022) that the CMIP6 GCMs have difficulties in reproducing sea ice in regions such as the Barents-Kara sea, and that the CMIP6 multi-model mean underestimates the Barents-Kara SIC negative trend in winter. They show that underestimation of the Gulf Stream surface warming is a likely reason for the too small Barents-Kara negative trend. The present results are consistent with this finding, as CNRM and NorESM underestimate the magnitude of the observed sea

https://doi.org/10.5194/egusphere-2026-1849
Preprint. Discussion started: 9 April 2026
© Author(s) 2026. CC BY 4.0 License.

ice decline. From the coupled regional models, HIRHAM–NAOSIM does not cover the Gulf Stream region between 30–80° W and 30–50° N as NAOSIM's southern border is at around 50° N, while RASM only partly covers the area in question. This means that the possible influence of remote North Atlantic warming, which has been shown to contribute to Barents–Kara sea ice decline (Yamagami et al., 2022), may only partly be represented in these regional model simulations, and would instead be included within their lateral forcing.

The two CMIP6 models chosen for this study represent high and low Barents-Kara sea warming according to the storyline analysis by Levine et al. (2024). Thus, they are models far from the multi-model mean and not necessarily the best CMIP6 model in terms of closeness to observations. NorESM is the model for low BK warming, and CNRM is the one for high BK warming. It is, however, surprising that neither of the two models shows a significant trend during the historical period, though they clearly differ in the future scenarios. The largest differences between the models during the period of 1991–2014 are that CNRM clearly underestimates the autumn sea ice extent and concentration, especially in the Kara Sea, while NorESM clearly overestimates it. NorESM also have a clearly higher sea ice thickness than CNRM (not shown), which might be the reason for its lower than average warming in the future projections.

Even though the Barents and Kara Seas are a relatively small (11%) part of the Arctic Ocean, they play a larger role than their size indicates for Arctic sea ice and the global climate (Peng et al., 2025). They have contributed to 30–40% of the Arctic winter sea ice loss in recent years (Onarheim et al., 2018; Liu et al., 2022), and the processes of ocean–sea-ice–atmosphere interaction in the region affect the ocean and sea ice further downstream. Models currently struggle to represent this region. One reason is resolution, as at least 0.25° resolution is needed to correctly simulate the ocean currents in the Barents Sea (Docquier et al., 2020), which is not the case in the CMIP6 models. However, as seen in this study, even higher resolution models struggle. Docquier et al. (2020) also found that the effect of increasing the resolution on ocean heat transport and March sea ice area in the Barents Sea differs between models, suggesting that more work is needed than simply increasing the resolution. Further model development is therefore required to better understand the drivers of the declining sea ice trends in the Barents and Kara Seas and to improve the representation of current trends in models in order to better predict future changes.

Code and data availability. RARE 1.15.2 (Carton and Chepurin, 2023) data was acquired through the UMD Ocean Climate Lab https://www2.atmos.umd.edu/~carton/index_files2/rare1.15.2_download.htm. TOPAZ4b data, was acquired from the CMEMS website https://doi.org/10.48670/moi-00007. ORAS5 (Zuo et al., 2019) was aquired from the Universität Hamburg website https://www.cen.uni-hamburg.de/icdc/data/ocean/easy-init-ocean/ecmwf-oras5.html. OSI-SAF data (EUMETSAT, 2022) is available at EUMETSAT https://doi.org/10.15770/EUM_SAF_OSI_0013. The NorESM2-MM and CNRM-ESM2-1 simulations are part of the World Climate Research Programme (WCRP)'s CMIP6 archived simulations, which can be found on the Earth System Grid Federation (ESGF, https://pcmdi.llnl.gov/CMIP6/, Lawrence Livermore National Laboratory, 2025). HIRHAM–NAOSIM data are available at the tape archive of the German Climate Computing Center (DKRZ) via https://hdl.handle.net/21.14106/a6d312c42d4501e75bd9de9186b323206ff5a65b (Dorn, 2024, dataset DKRZ_LTA_049_ds00009). RASM data was acquired from Naval Postgraduate School, Monterey, CA, United States, through WM. Code for producing plots of this manuscript as well as a subset of the data needed for this can be found at https://doi.org/10.5281/zenodo.19328005 (Äijälä, 2026)

https://doi.org/10.5194/egusphere-2026-1849
Preprint. Discussion started: 9 April 2026
© Author(s) 2026. CC BY 4.0 License.

Appendix A: Additional figures

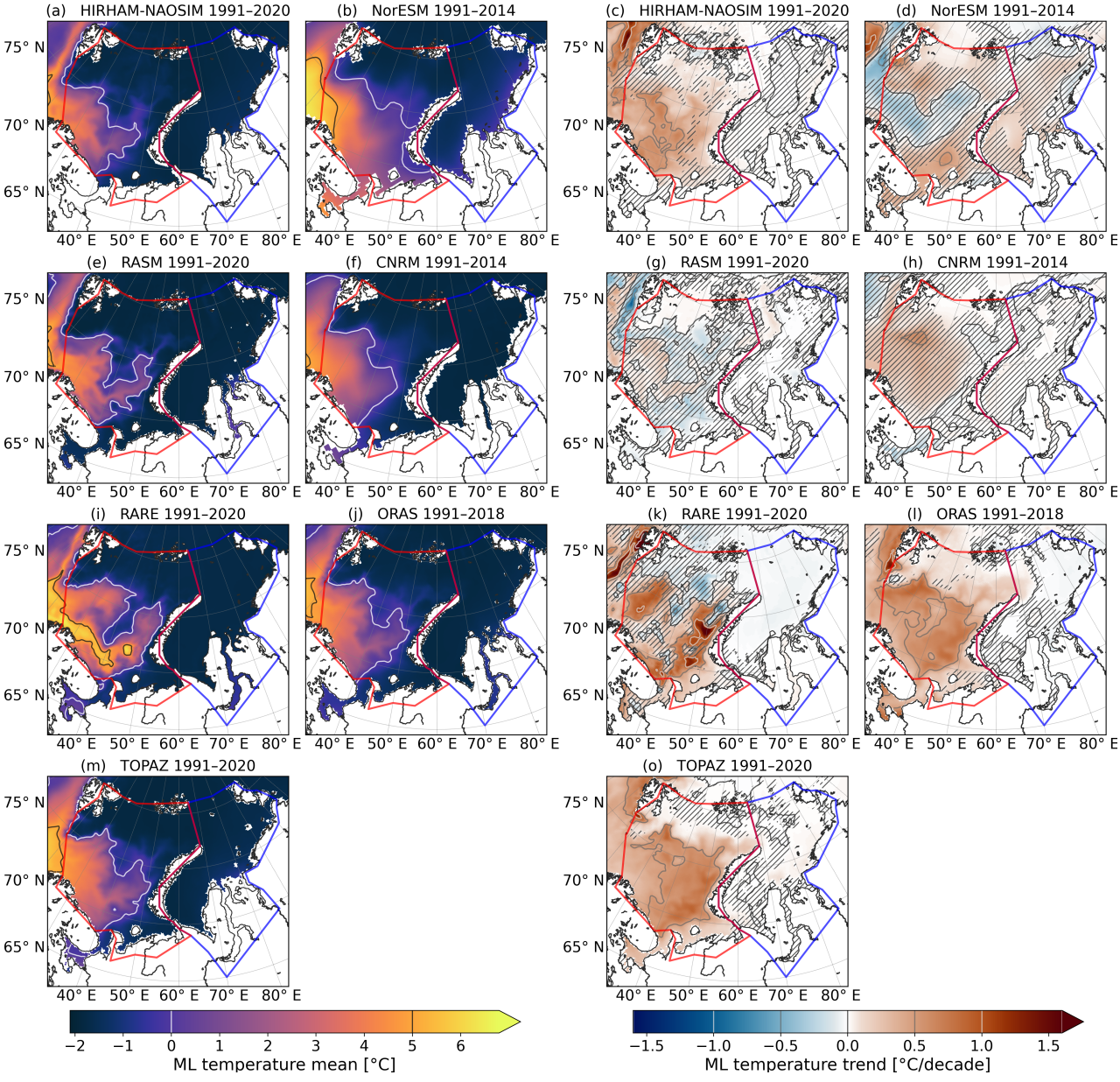


Figure A1. Average of mean ML temperature (left) and trend (right) of all the datasets in spring (MAM) over the whole period.

https://doi.org/10.5194/egusphere-2026-1849
Preprint. Discussion started: 9 April 2026
© Author(s) 2026. CC BY 4.0 License.

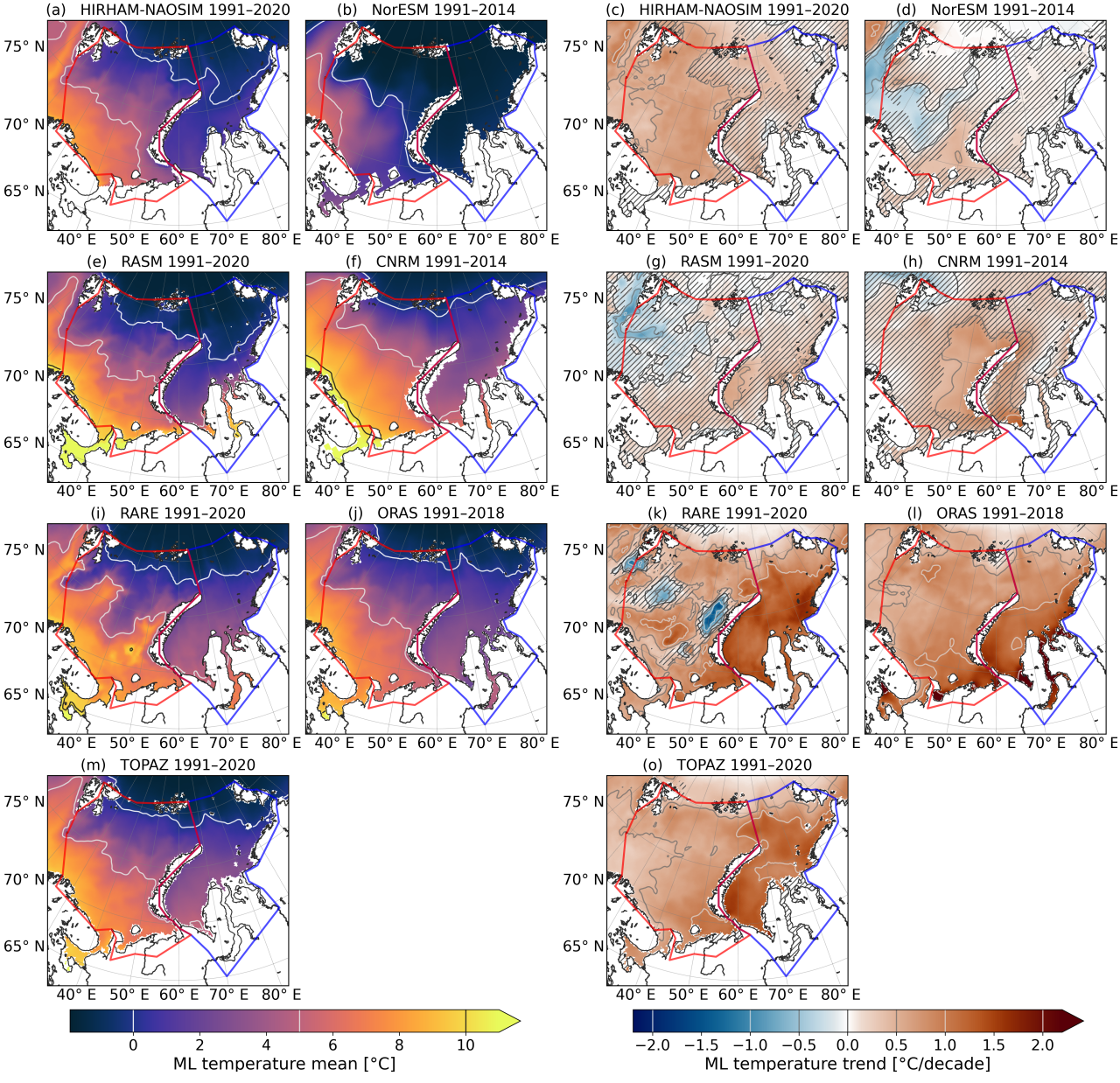


Figure A2. Average of mean ML temperature (left) and trend (right) of all the datasets in autumn (ASO) over the whole period.

https://doi.org/10.5194/egusphere-2026-1849
Preprint. Discussion started: 9 April 2026
© Author(s) 2026. CC BY 4.0 License.

A1

Author contributions. **C. Ä.:** Conceptualization, Methodology, Software, Formal analysis, Investigation, Writing - Original Draft, Writing - Review & Editing, Visualization **L. G.-L.:** Conceptualization, Writing - Original Draft, Writing - Review & Editing **W. D.:** Conceptualization, Resources, Writing - Review & Editing, Project administration, Funding acquisition **S. K. L.:** Conceptualization, Writing - Review & Editing, Supervision, Project administration, Funding acquisition **W. M.:** Conceptualization, Resources, Writing - Review & Editing **P. U.:** Conceptualization, Writing - Original Draft, Writing - Review & Editing, Supervision, Project administration, Funding acquisition.

Competing interests. The authors declare that they have no conflict of interest.

Acknowledgements. This study was undertaken as part of the European Union's Horizon 2020 research and innovation program under grant agreement no. 101003590 (PolarRES project; https://polarres.eu). The authors thank the European Commission for facilitating this research. The work was also supported by the Research Council of Finland (contract 364876). WD also acknowledge the funding by the Deutsche Forschungsgemeinschaft (DFG, German Research Foundation) project 268020496 TRR 172, within the Transregional Collaborative Research Center "ArctiC Amplification: Climate Relevant Atmospheric and SurfaCe Processes, and Feedback Mechanisms (AC)^3". The authors wish to acknowledge CSC – IT Center for Science, Finland, for computational resources. This work also used resources of the Deutsches Klimarechenzentrum (DKRZ) under project ID aa0049. This study has been conducted using E.U. Copernicus Marine Service Information (https://doi.org/10.48670/moi-00007) ChatGPT and Microsoft Copilot assisted with initial data visualization code and with light language editing of an earlier draft. All code was reviewed and further refined by CÄ.

https://doi.org/10.5194/egusphere-2026-1849
Preprint. Discussion started: 9 April 2026
© Author(s) 2026. CC BY 4.0 License.

References

Asbjørnsen, H., Årthun, M., Skagseth, , and Eldevik, T.: Mechanisms Underlying Recent Arctic Atlantification, Geophysical Research Letters, 47, e2020GL088 036, https://doi.org/10.1029/2020GL088036, 2020.

Aue, L., Röntgen, L., Dorn, W., Uotila, P., Vihma, T., Spreen, G., and Rinke, A.: Impact of three intense winter cyclones on the sea ice cover in the Barents Sea: A case study with a coupled regional climate model, Frontiers in Earth Science, 11, https://doi.org/10.3389/feart.2023.1112467, 2023.

Balmaseda, M., Hernandez, F., Storto, A., Palmer, M., Alves, O., Shi, L., Smith, G., Toyoda, T., Valdivieso, M., Barnier, B., Behringer, D., Boyer, T., Chang, Y.-S., Chepurin, G., Ferry, N., Forget, G., Fujii, Y., Good, S., Guinehut, S., Haines, K., Ishikawa, Y., Keeley, S., Köhl, A., Lee, T., Martin, M., Masina, S., Masuda, S., Meyssignac, B., Mogensen, K., Parent, L., Peterson, K., Tang, Y., Yin, Y., Vernieres, G., Wang, X., Waters, J., Wedd, R., Wang, O., Xue, Y., Chevallier, M., Lemieux, J.-F., Dupont, F., Kuragano, T., Kamachi, M., Awaji, T., Caltabiano, A., Wilmer-Becker, K., and Gaillard, F.: The Ocean Reanalyses Intercomparison Project (ORA-IP), Journal of Operational Oceanography, 8, 80–97, https://doi.org/10.1080/1755876X.2015.1022329, 2015.

Carton, J. A. and Chepurin, G. A.: RARE: The Regional Arctic Reanalysis, Journal of Climate, 36, 2333–2348, https://doi.org/10.1175/JCLI-D-22-0340.1, 2023.

Cassano, J. J., DuVivier, A., Roberts, A., Abel, M. R., Seefeldt, M., Brunke, M., Craig, A., Fisel, B., Gutowski, W., Hamman, J., Higgins, M., Maslowski, W., Nijssen, B., Osinski, R., and Zeng, X.: Development of the Regional Arctic System Model (RASM): Near-Surface Atmospheric Climate Sensitivity, Journal of Climate, 30, 5729–5753, https://doi.org/10.1175/JCLI-D-15-0775.1, 2017.

Chassignet, E. P., Smith, L. T., Halliwell, G. R., and Bleck, R.: North Atlantic Simulations with the Hybrid Coordinate Ocean Model (HYCOM): Impact of the Vertical Coordinate Choice, Reference Pressure, and Thermobaricity, Journal of Physical Oceanography, 33, 2504–2526, https://doi.org/10.1175/1520-0485(2003)033<2504:NASWTH>2.0.CO;2, 2003.

Chatterjee, S., Semmler, T., Screen, J., Furevik, T., Selivanova, J., Raj, R. P., Murukesh, N., and Ravichandran, A. M.: Atmosphere–Ocean–Sea Ice Feedbacks Sustain Recent Barents Sea Ice Loss despite Cooler Atlantic Water Inflow, Journal of Climate, 37, 6519–6532, https://doi.org/10.1175/JCLI-D-24-0020.1, 2024.

Comiso, J. C.: Abrupt decline in the Arctic winter sea ice cover, Geophysical Research Letters, 33, https://doi.org/10.1029/2006GL027341, 2006.

Docquier, D., Fuentes-Franco, R., Koenigk, T., and Fichefet, T.: Sea Ice—Ocean Interactions in the Barents Sea Modeled at Different Resolutions, Frontiers in Earth Science, 8, https://doi.org/10.3389/feart.2020.00172, 2020.

Donlon, C. J., Martin, M., Stark, J., Roberts-Jones, J., Fiedler, E., and Wimmer, W.: The Operational Sea Surface Temperature and Sea Ice Analysis (OSTIA) system, Remote Sensing of Environment, 116, 140–158, https://doi.org/10.1016/j.rse.2010.10.017, 2012.

Dorn, W.: HIRHAM–NAOSIM simulations for the period 1979–2021 with ice–ocean initialization from ORAS5 (P3), DOKU at DKRZ [data set], https://hdl.handle.net/21.14106/a6d312c42d4501e75bd9de9186b323206ff5a65b, 2024.

Dorn, W., Rinke, A., Köberle, C., Dethloff, K., and Gerdes, R.: Evaluation of the Sea-Ice Simulation in the Upgraded Version of the Coupled Regional Atmosphere-Ocean- Sea Ice Model HIRHAM–NAOSIM 2.0, Atmosphere, 10, 431, https://doi.org/10.3390/atmos10080431, 2019.

Duan, C., Dong, S., and Wang, Z.: New insights into the quantitative description of seasonal sea ice variability process in the semi-closed Kara Sea, Regional Studies in Marine Science, 32, https://doi.org/10.1016/j.rsma.2019.100856, 2019a.

https://doi.org/10.5194/egusphere-2026-1849
Preprint. Discussion started: 9 April 2026
© Author(s) 2026. CC BY 4.0 License.

Duan, C., Dong, S., Xie, Z., and Wang, Z.: Temporal variability and trends of sea ice in the Kara Sea and their relationship with atmospheric factors, Polar Science, 20, 136–147, https://doi.org/10.1016/j.polar.2019.03.002, 2019b.

Dörr, J., Årthun, M., Docquier, D., Li, C., and Eldevik, T.: Causal Links Between Sea-Ice Variability in the Barents-Kara Seas and Oceanic and Atmospheric Drivers, Geophysical Research Letters, 51, e2024GL108 195, https://doi.org/10.1029/2024GL108195, 2024.

EUMETSAT: OSI SAF Global sea ice concentration climate data record 1978-2020, https://doi.org/10.15770/EUM_SAF_OSI_0013, 2022.

Eyring, V., Bony, S., Meehl, G. A., Senior, C. A., Stevens, B., Stouffer, R. J., and Taylor, K. E.: Overview of the Coupled Model Intercomparison Project Phase 6 (CMIP6) experimental design and organization, Geoscientific Model Development, 9, 1937–1958, https://doi.org/10.5194/gmd-9-1937-2016, 2016.

Goessling, H. F., Tietsche, S., Day, J. J., Hawkins, E., and Jung, T.: Predictability of the Arctic sea ice edge, Geophysical Research Letters, 43, 1642–1650, https://doi.org/10.1002/2015GL067232, 2016.

Goosse, H., Kay, J. E., Armour, K. C., Bodas-Salcedo, A., Chepfer, H., Docquier, D., Jonko, A., Kushner, P. J., Lecomte, O., Massonnet, F., Park, H.-S., Pithan, F., Svensson, G., and Vancoppenolle, M.: Quantifying climate feedbacks in polar regions, Nature Communications, 9, 1919, https://doi.org/10.1038/s41467-018-04173-0, 2018.

Gouretski, V. and Reseghetti, F.: On depth and temperature biases in bathythermograph data: Development of a new correction scheme based on analysis of a global ocean database, Deep Sea Research Part I: Oceanographic Research Papers, 57, 812–833, https://doi.org/10.1016/j.dsr.2010.03.011, 2010.

Gurvan, M., Bourdallé-Badie, R., Bouttier, P.-A., Bricaud, C., Bruciaferri, D., Calvert, D., Chanut, J., Clementi, E., Coward, A., Delrosso, D., Ethé, C., Flavoni, S., Graham, T., Harle, J., Iovino, D., Lea, D., Lévy, C., Lovato, T., Martin, N., Masson, S., Mocavero, S., Paul, J., Rousset, C., Storkey, D., Storto, A., and Vancoppenolle, M.: NEMO ocean engine, https://doi.org/10.5281/zenodo.1472492, 2017.

Hersbach, H., Bell, B., Berrisford, P., Hirahara, S., Horányi, A., Muñoz-Sabater, J., Nicolas, J., Peubey, C., Radu, R., Schepers, D., Simmons, A., Soci, C., Abdalla, S., Abellan, X., Balsamo, G., Bechtold, P., Biavati, G., Bidlot, J., Bonavita, M., De Chiara, G., Dahlgren, P., Dee, D., Diamantakis, M., Dragani, R., Flemming, J., Forbes, R., Fuentes, M., Geer, A., Haimberger, L., Healy, S., Hogan, R. J., Hólm, E., Janisková, M., Keeley, S., Laloyaux, P., Lopez, P., Lupu, C., Radnoti, G., de Rosnay, P., Rozum, I., Vamborg, F., Villaume, S., and Thépaut, J.-N.: The ERA5 global reanalysis, Quarterly Journal of the Royal Meteorological Society, 146, 1999–2049, https://doi.org/10.1002/qj.3803, 2020.

Ingvaldsen, R. B., Assmann, K. M., Primicerio, R., Fossheim, M., Polyakov, I. V., and Dolgov, A. V.: Physical manifestations and ecological implications of Arctic Atlantification, Nature Reviews Earth & Environment, 2, 874–889, https://doi.org/10.1038/s43017-021-00228-x, 2021.

International Hydrographic Organization, I. H. O. and Sieger, R.: Limits of oceans and seas in digitized, machine readable form, https://doi.org/10.1594/PANGAEA.777975, 2012.

Kumar, A., Yadav, J., and Mohan, R.: Spatio-temporal change and variability of Barents-Kara sea ice, in the Arctic: Ocean and atmospheric implications, Science of The Total Environment, 753, 142 046, https://doi.org/10.1016/j.scitotenv.2020.142046, 2021.

Levine, X. J., Williams, R. S., Marshall, G., Orr, A., Seland Graff, L., Handorf, D., Karpechko, A., Köhler, R., Wijngaard, R. R., Johnston, N., Lee, H., Nieradzik, L., and Mooney, P. A.: Storylines of summer Arctic climate change constrained by Barents–Kara seas and Arctic tropospheric warming for climate risk assessment, Earth System Dynamics, 15, 1161–1177, https://doi.org/10.5194/esd-15-1161-2024, 2024.

Li, M., Ke, C., Cheng, B., Shen, X., He, Y., and Sha, D.: The Roles of Sea Ice Export, Atmospheric and Oceanic Factors in the Seasonal and Regional Variability of Arctic Sea Ice during 1979–2020, Remote Sensing, 14, https://doi.org/10.3390/rs14040904, 2022.

https://doi.org/10.5194/egusphere-2026-1849
Preprint. Discussion started: 9 April 2026
© Author(s) 2026. CC BY 4.0 License.



Lind, S., Ingvaldsen, R. B., and Furevik, T.: Arctic warming hotspot in the northern Barents Sea linked to declining sea-ice import, Nature Climate Change, 8, 634–639, https://doi.org/10.1038/s41558-018-0205-y, 2018.

Lindsay, R. W. and Zhang, J.: Assimilation of ice concentration in an ice–ocean model, J. Atmos. Oceanic Technol., 23, 742–749, 2006.

Liu, Y., Losch, M., Tremblay, L. B., and Janout, M.: Landfast ice in the Kara Sea stabilizes the Arctic halocline and may slow down Atlantification of the Eurasian Basin, Communications Earth and Environment, 6, https://doi.org/10.1038/s43247-025-02360-8, 2025.

Liu, Z., Risi, C., Codron, F., Jian, Z., Wei, Z., He, X., Poulsen, C. J., Wang, Y., Chen, D., Ma, W., Cheng, Y., and Bowen, G. J.: Atmospheric forcing dominates winter Barents-Kara sea ice variability on interannual to decadal time scales, Proceedings of the National Academy of Sciences, 119, e2120770 119, https://doi.org/10.1073/pnas.2120770119, 2022.

Onarheim, I. H., Eldevik, T., Smedsrud, L. H., and Stroeve, J. C.: Seasonal and Regional Manifestation of Arctic Sea Ice Loss, Journal of Climate, 31, 4917–4932, https://doi.org/10.1175/JCLI-D-17-0427.1, 2018.

Peng, Y., Duan, A., Shen, Z., Wei, J., and Cao, S.: Emergent Constraint on CMIP6 Model Projections of Winter Ice-Free Periods in the Barents–Kara Sea, Geophysical Research Letters, 52, e2025GL117 660, https://doi.org/10.1029/2025GL117660, 2025.

Salas Mélia, D.: A global coupled sea ice–ocean model, Ocean Modelling, 4, 137–172, https://doi.org/10.1016/S1463-5003(01)00015-4, 2002.

Sallée, J.-B., Wienders, N., Speer, K., and Morrow, R.: Formation of Subantarctic Mode Water in the southeastern Indian Ocean, Ocean Dynamics, 56, 525–542, https://doi.org/10.1007/s10236-005-0054-x, 2006.

Sallée, J.-B., Shuckburgh, E., Bruneau, N., Meijers, A. J. S., Bracegirdle, T. J., and Wang, Z.: Assessment of Southern Ocean mixed-layer depths in CMIP5 models: Historical bias and forcing response, Journal of Geophysical Research: Oceans, 118, 1845–1862, https://doi.org/10.1002/jgrc.20157, 2013.

Seland, , Bentsen, M., Olivié, D., Toniazzo, T., Gjermundsen, A., Graff, L. S., Debernard, J. B., Gupta, A. K., He, Y.-C., Kirkevåg, A., Schwinger, J., Tjiputra, J., Aas, K. S., Bethke, I., Fan, Y., Griesfeller, J., Grini, A., Guo, C., Ilicak, M., Karset, I. H. H., Landgren, O., Liakka, J., Moseid, K. O., Nummelin, A., Spensberger, C., Tang, H., Zhang, Z., Heinze, C., Iversen, T., and Schulz, M.: Overview of the Norwegian Earth System Model (NorESM2) and key climate response of CMIP6 DECK, historical, and scenario simulations, Geoscientific Model Development, 13, 6165–6200, https://doi.org/10.5194/gmd-13-6165-2020, 2020.

Shabanov, P., Osadchiev, A., Shabanova, N., and Ogorodov, S.: Decline in Ice Coverage and Ice-Free Period Extension in the Kara and Laptev Seas during 1979–2022, Remote Sensing, 16, https://doi.org/10.3390/rs16111875, 2024.

Shepherd, T. G., Boyd, E., Calel, R. A., Chapman, S. C., Dessai, S., Dima-West, I. M., Fowler, H. J., James, R., Maraun, D., Martius, O., Senior, C. A., Sobel, A. H., Stainforth, D. A., Tett, S. F. B., Trenberth, K. E., van den Hurk, B. J. J. M., Watkins, N. W., Wilby, R. L., and Zenghelis, D. A.: Storylines: an alternative approach to representing uncertainty in physical aspects of climate change, Climatic Change, 151, 555–571, https://doi.org/10.1007/s10584-018-2317-9, 2018.

Skagseth, , Furevik, T., Ingvaldsen, R., Loeng, H., Mork, K. A., Orvik, K. A., and Ozhigin, V.: Volume and Heat Transports to the Arctic Ocean Via the Norwegian and Barents Seas, in: Arctic–Subarctic Ocean Fluxes: Defining the Role of the Northern Seas in Climate, edited by Dickson, R. R., Meincke, J., and Rhines, P., pp. 45–64, Springer Netherlands, Dordrecht, ISBN 978-1-4020-6774-7, https://doi.org/10.1007/978-1-4020-6774-7_3, 2008.

Smedsrud, L. H., Esau, I., Ingvaldsen, R. B., Eldevik, T., Haugan, P. M., Li, C., Lien, V. S., Olsen, A., Omar, A. M., Otterå, O. H., Risebrobakken, B., Sandø, A. B., Semenov, V. A., and Sorokina, S. A.: The Role of the Barents Sea in the Arctic Climate System, Reviews of Geophysics, 51, 415–449, https://doi.org/10.1002/rog.20017, 2013.

https://doi.org/10.5194/egusphere-2026-1849
Preprint. Discussion started: 9 April 2026
© Author(s) 2026. CC BY 4.0 License.

Storto, A., Alvera-Azcárate, A., Balmaseda, M. A., Barth, A., Chevallier, M., Counillon, F., Domingues, C. M., Drevillon, M., Drillet, Y., Forget, G., Garric, G., Haines, K., Hernandez, F., Iovino, D., Jackson, L. C., Lellouche, J.-M., Masina, S., Mayer, M., Oke, P. R., Penny, S. G., Peterson, K. A., Yang, C., and Zuo, H.: Ocean Reanalyses: Recent Advances and Unsolved Challenges, Frontiers in Marine Science, 6, https://doi.org/10.3389/fmars.2019.00418, 2019.

Stroeve, J. and Notz, D.: Changing state of Arctic sea ice across all seasons, Environmental Research Letters, 13, 103 001, https://doi.org/10.1088/1748-9326/aade56, 2018.

Séférian, R., Nabat, P., Michou, M., Saint-Martin, D., Voldoire, A., Colin, J., Decharme, B., Delire, C., Berthet, S., Chevallier, M., Sénési, S., Franchisteguy, L., Vial, J., Mallet, M., Joetzjer, E., Geoffroy, O., Guérémy, J.-F., Moine, M.-P., Msadek, R., Ribes, A., Rocher, M., Roehrig, R., Salas-y Mélia, D., Sanchez, E., Terray, L., Valcke, S., Waldman, R., Aumont, O., Bopp, L., Deshayes, J., Éthé, C., and Madec, G.: Evaluation of CNRM Earth System Model, CNRM-ESM2-1: Role of Earth System Processes in Present-Day and Future Climate, Journal of Advances in Modeling Earth Systems, 11, 4182–4227, https://doi.org/10.1029/2019MS001791, 2019.

Uotila, P., Goosse, H., Haines, K., Chevallier, M., Barthélemy, A., Bricaud, C., Carton, J., Fučkar, N., Garric, G., Iovino, D., Kauker, F., Korhonen, M., Lien, V. S., Marnela, M., Massonnet, F., Mignac, D., Peterson, K. A., Sadikni, R., Shi, L., Tietsche, S., Toyoda, T., Xie, J., and Zhang, Z.: An assessment of ten ocean reanalyses in the polar regions, Climate Dynamics, 52, 1613–1650, https://doi.org/10.1007/s00382-018-4242-z, 2019.

Xie, J. and Bertino, L.: PRODUCT USER MANUAL For Arctic Ocean Physical Reanalysis Product, 2025.

Xie, J., Bertino, L., Counillon, F., Lisæter, K. A., and Sakov, P.: Quality assessment of the TOPAZ4 reanalysis in the Arctic over the period 1991–2013, Ocean Science, 13, 123–144, https://doi.org/10.5194/os-13-123-2017, 2017.

Xie, J., Raj, R. P., Bertino, L., Martínez, J., Gabarró, C., and Catany, R.: Assimilation of sea surface salinities from SMOS in an Arctic coupled ocean and sea ice reanalysis, Ocean Science, 19, 269–287, https://doi.org/10.5194/os-19-269-2023, 2023.

Xiong, Z., Yan, Y., Xu, J., Yao, C., and Xu, Y.: Comparative analysis of sea ice conditions in five reanalysis datasets along the Northern Sea Route, Ocean Dynamics, 75, 37, https://doi.org/10.1007/s10236-025-01684-5, 2025.

Yamagami, Y., Watanabe, M., Mori, M., and Ono, J.: Barents-Kara sea-ice decline attributed to surface warming in the Gulf Stream, Nature Communications, 13, 3767, https://doi.org/10.1038/s41467-022-31117-6, 2022.

Zhang, Y.-F., Bushuk, M., Winton, M., Hurlin, B., Yang, X., Delworth, T., and Jia, L.: Assimilation of Satellite-Retrieved Sea Ice Concentration and Prospects for September Predictions of Arctic Sea Ice, Journal of Climate, 34, 2107–2126, https://doi.org/10.1175/JCLI-D-20-0469.1, 2021.

Zuo, H., Balmaseda, M. A., Tietsche, S., Mogensen, K., and Mayer, M.: The ECMWF operational ensemble reanalysis–analysis system for ocean and sea ice: a description of the system and assessment, Ocean Science, 15, 779–808, https://doi.org/10.5194/os-15-779-2019, 2019.

Äijälä, C.: Code for Barents and Kara Seas model and reanalysis comparision analysis, https://doi.org/10.5281/zenodo.19328005, 2026.

Årthun, M., Eldevik, T., Smedsrud, L. H., Skagseth, , and Ingvaldsen, R. B.: Quantifying the Influence of Atlantic Heat on Barents Sea Ice Variability and Retreat in: Journal of Climate Volume 25 Issue 13 (2012), Journal of Climate, 25, https://doi.org/10.1175/JCLI-D-11-00466.1, 2012.